RADIATIVE CHARACTERISTICS OF CLOUDS IN THE INFRARED

by

R. E. Samuelson

Goddard Space Flight Center
Aeronomy and Meteorology Division
Greenbelt, Maryland

SUBJECT CATEGORIES FOR GODDARD JOURNAL

(To be used for classifying all NASA publications, journal articles, and other papers for inclusion in the Goddard Journal.)

Part A – Space Sciences

A 1. Astronomy and Astrophysics
A 2. Celestial Mechanics and Geodesy
A 3. Solar Physics
A 4. Ionosphere and Radio Physics
A 5. Fields and Particles
A 6. Planetology
A 7. Planetary Atmospheres
A 8. General (subjects not clearly belonging in any of categories 1-7)

Part B – Space Technology

B 1. Projects and Programs
B 2. Space Dynamics and Control Systems
B 3. Spacecraft and Subsystems
B 4. Vehicle Technology
B 5. Sounding Rockets
B 6. Sensors
B 7. General Electronics
B 8. Environmental Testing
B 9. Tracking Systems
B 10. General (subjects not clearly belonging in any of categories 1-9)

RADIATIVE CHARACTERISTICS OF CLOUDS

IN THE INFRARED

by

R. E. Samuelson
NASA/Goddard Space Flight Center
Greenbelt, Maryland

N66 18358

Equations of transfer which include the effects of thermal emission and anisotropic multiple scattering are solved by the method of discrete ordinates, and the angular distribution and net flux of outgoing radiation are calculated for various model clouds and cloudy atmospheres. The cloud models adopted are plane-parallel and of normal optical thickness τ_c = 0.1, 0.5, and ∞. The principal wavenumber intervals chosen for examination are centered about 889.5 cm^{-1} and 1173.5 cm^{-1}. The contributions of the outgoing radiation field at the top of the atmosphere, due to diffuse reflection, diffuse transmission, direct transmission, and thermal emission are traced out in detail for each model cloudy atmosphere. Based on the explicit outgoing radiation field predicted for each model, the following four general conclusions are reached: (1) Limb darkening is considerable at very large zenith angles, and especially pronounced for thin clouds which are much cooler than the effective radiating layer below them. (2) A considerable flux surplus in the infrared window compared with the rest of the infrared spectrum is predicted for atmospheres containing cold, thin clouds. (3) A modest flux deficit in the infrared window is predicted for atmospheres containing very extensive warm, thick clouds. (4) For the same cloud top temperature, the outgoing radiation fields are virtually the same for an isothermal cloud and a cloud having a realistic temperature gradient of 5°C km^{-1}. All conclusions have to be modified if multiple cloud decks and cloud configurations other than plane-parallel are considered.

author

1. Introduction

A knowledge of the transfer of infrared radiation in and through clouds is of fundamental importance in the overall investigation of radiative transfer in the Earth's atmosphere. It will be the purpose of this paper to further progress toward placing the physical understanding of the radiative characteristics of water clouds on a more nearly equal footing with that of the clear atmosphere. To this end we shall be concerned with: a) the numerical determination of the role and importance of diffuse reflection and transmission and of thermal emission in and from clouds, b) the angular distribution and net flux of outgoing radiation in selected wavenumber intervals at the top of certain model cloudy atmospheres, c) an interpretation of the main radiative features in terms of the relevant physical parameters, and d) a qualitative extrapolation to probable radiative characteristics of clouds and cloudy atmospheres at other regions of the spectrum and for other physical situations not explicitly covered by the computations in this paper.

In order to maintain physical rigor it is imperative to eliminate approximations based on intuition insofar as possible in the mathematical formulation of the general problem. It is further required to maintain as much generality in the formulation as possible in order that the range of validity not be overly restrictive. These objectives require solutions to rather sophisticated equations of radiative transfer; a powerful technique developed primarily by Chandrasekhar for the purpose of obtaining these solutions will be the one exploited here. A full account of the Mie theory for single scattering and the theory of the transfer of radiation through the surrounding gaseous atmosphere will be included in the computations which are required in order to fix the boundary conditions and describe the microscopic scattering processes. A complete description of multiple scattering processes then follows from the solutions to the relevant equations of radiative transfer.

2. The Equation of Transfer

The cloud models adopted are plane-parallel and of arbitrary normal optical thickness. The particle size distribution is maintained independent of optical depth, although the mass distribution with height is left arbitrary. Each mass element in the cloud is assumed to emit radiation thermally in accordance with Kirchhoff's law and scatter radiation in accordance with the Mie theory. The temperature is assumed to be a monotonic function of the optical depth and independent of horizontal displacement. The (thermal) radiation field is assumed to have axial symmetry about any normal to the plane of stratification; this immediately eliminates any outside <u>discrete</u> source of radiation (e.g. the sun) from consideration. The state of polarization of the radiation field is neglected, thereby reducing the transfer equation to a scalar equation. Since we are interested in both the magnitude and angular distribution of radiation, the specific intensity is our choice for the dependent variable. In order to maintain as much physical rigor as possible, no quantities which are not strictly independent of the radiation field are allowed to enter the equation as free parameters.

It has been shown by Samuelson (1964) that the basic equation of transfer which satisfies these requirements is of the form

$$\mu \frac{dI(\tau,\mu)}{d\tau} = I(\tau,\mu) - \frac{1}{2}\int_{-1}^{+1} p(\mu,\mu')\, I(\tau,\mu')\, d\mu' - (1-\varpi_0)\, B(\tau) , \tag{2.1}$$

where the relevant parameters are defined below.

The specific intensity $I(\tau,\mu)$ is the rate at which radiant energy confined to a unit solid angle and a unit wave-number interval crosses (at a level τ) a unit surface area normal to the direction of propagation. The direction cosine μ specifies the cosine of the (zenith) angle between the direction of propagation and the outward normal to the plane of stratification.

The normal optical depth τ is defined by

$$\tau = -\int_{z_0}^{z} N_0 \chi_E \, dz \tag{2.2}$$

where z_0 is the height of the cloud top, z is the height of the level of interest and N_0 is the total number of particles per unit volume. The effective cross-sections per particle for extinction (χ_E), absorption (χ_A), and scattering (χ_S) are defined by

$$\chi_j = \int_0^\infty Q_j \pi r^2 D(r) dr \quad (j = E, A, S) \tag{2.3}$$

where Q_j ($j = E, A, S$) are respectively the Mie efficiency factors for extinction, absorption, and scattering for particles of radius r. D(r) is the ratio of the number of particles per unit volume per unit radius range (centered about r) to N_0 , i.e. the particle size distribution function.

The integrated phase function for single scattering is defined by

$$p(\mu,\mu') = \frac{1}{2\pi}\int_0^{2\pi}\left[\frac{\int_0^{\infty} Q_s \pi r^2 D(r)\, p_r(\cos\Theta)\, dr}{\int_0^{\infty} Q_s \pi r^2 D(r)\, dr}\right] d(\phi'-\phi), \tag{2.4}$$

where $p_r(\cos\Theta)$ is the phase function for single scattering through the angle Θ for particles of radius r. It can be shown from spherical trigonometry that Θ may be expressed in terms of the coordinate angles θ, θ', ϕ, ϕ' through the relation

$$\cos\Theta = \cos\theta\cos\theta' + \sin\theta\sin\theta'\cos(\phi'-\phi), \tag{2.5}$$

where $\mu' = \cos\theta'$ and $\mu = \cos\theta$ are respectively the direction cosines of the incident and scattered radiation referred to the outward normal to the plane of stratification, and ϕ and ϕ' are the corresponding azimuthal angles measured in the plane of stratification.

$p(\mu,\mu')$ is normalized to the albedo for single scattering, $\tilde{\omega}_0$, defined by

$$\tilde{\omega}_0 = \frac{\int_0^\infty Q_S \pi r^2 D(r)\, dr}{\int_0^\infty Q_E \pi r^2 D(r)\, dr} \quad . \tag{2.6}$$

The quantities Q_E, Q_S, and $p_r(\cos\theta)$ may be calculated from the Mie theory.

B(τ), the Planck function in intensity units, is assumed to be a monotonic function of τ alone.

It should be noted that all derived quantities in (2.1) are functions of the wavenumber ν; thus (2.1) is valid only over a wavenumber interval small enough such that the derived quantities remain sensibly constant across the interval. It should further be noted at this point that $I(\tau,\mu)$ refers to the total radiation field, and thus implicitly includes all radiation from the ground and bounding atmosphere which has been transmitted directly to the level τ without suffering any intermediate scattering and/or absorption and emission processes.

3. Input Data

Certain input data are required before the parameters Q_E, Q_S, and $p_r(\cos\Theta)$ can be calculated. These data include the complex index of refraction of water, $\tilde{n} = n - ik$, the particle size distribution, D(r), and the wavenumber intervals of interest, $\Delta\nu$.

Figure 1 is a plot of the real (n) and imaginary (k) parts of $\tilde{n}$ vs. wavenumber ν. The curves are fitted to the data published by Centano, Johnson and Terrell, Herman, and Stephens as listed by Penndorf (1963). The section of the k vs. ν curve for the range (1050 cm$^{-1} \leq \nu \leq$ 1450 cm^{-1}) was obtained by rather arbitrarily weighting the more recent data by Herman and Stephens twice as heavily as the older data. This is a very critical section of the curve, since only a modest shift of the value of k will affect considerably the relative amount of absorption calculated.

The shaded portions of the figure indicate the wavenumber intervals which will be considered in this paper. Table 1 gives the range ($\nu_{min} \leq \nu \leq \nu_{max}$) and the mean ($\nu = \bar{\nu}$) of these intervals in inverse centimeters.

Table 1. Wavenumber intervals ($\nu_{min} \leq \nu \leq \nu_{max}$) and mean ($\bar{\nu}$) used in the computations.

Interval	ν_{min} (cm^{-1})	ν_{max} (cm^{-1})	$\bar{\nu}$ (cm^{-1})
1	475	500	487.5
2	871	908	889.5
3	1149	1198	1173.5
4	1425	1450	1437.5

The first two intervals were selected to be representative of the highest and lowest values of n. The last two values were selected for the purpose of testing the region of the spectrum where κ is a minimum.

The particle size distributions considered are taken (with minor modifications) from Neiburger (1949) and are represented in Figures 2a-2d. The narrower distribution, $D_1(r)$, centered about $d \approx 17\mu$ is representative of California stratus, excluding the base of the cloud; the broader distribution, $D_2(r)$ is representative of the base.

The graphs of Q_E and Q_A are superposed over D(r). These values, as well as all subsequent Mie scattering parameters, were obtained from a program furnished to the author by B. Donn and T. Michels of the Theoretical Division, Goddard Space Flight Center. The actual computations were performed on the IBM 7094 electronic computer. All minor wiggles in the calculated curves have been suppressed.

Four points should be mentioned: a) Decreasing the wavenumber has the effect of spreading the curves out to the right, b) increasing κ has the effect of increasing Q_A, c) increasing $\tilde{n}$ has the effect of increasing Q_E, and d) decreasing κ beyond a certain point has the effect of magnifying the oscillatory nature of $Q_S = Q_E - Q_A$.

In general every mass element in a cloud will extinguish (absorb and/or scatter) incident radiation at a rate in accordance with an effective cross-section for extinction which depends upon the absorption properties of the pervading gaseous atmosphere as well as the absorption and scattering properties of the particles present. Define g to be the probability that the incident radiation which is extinguished is extinguished by the particles. It can be shown (Samuelson, 1964) that, if g is independent of τ , equations (2.1) - (2.2) remain valid simply by replacing $\tilde{\omega}_0$ with $g\,\tilde{\omega}_0$ and N_0 with $\frac{1}{g} N_0$.

Deviations of g from unity in the wavenumber intervals centered about $\bar{\nu}$ = 487.5 cm^{-1} and $\bar{\nu}$ = 1437.5 cm^{-1} are due almost exclusively to absorption by water vapor. The exact amounts of these deviations depend very critically upon the absolute humidity. To further complicate matters the water vapor spectrum is extremely variable over very small intervals of wavenumber, and the transmission functions over these intervals are correspondingly far removed from simple exponentials. Hence, $g\tilde{\omega}_0$, and therefore also $p(\mu,\mu')$ are functions of τ , and the equation of transfer cannot be treated correctly by the method used in this paper.

In order to obtain an approximate idea of how water vapor affects $\tilde{\omega}_0$, transmission functions ($\mathcal{T}$) were calculated for various thicknesses of atmosphere containing saturation mixing ratios of water vapor. The two sets of values of the mean pressure and temperature used were [P = 950 mb; T = 287 K] and [P = 417 mb; T = 259 K] and the increments of thickness of all layers were restricted to those which correspond to pressure increments of between one and five millibars. An attempt was then made to determine an empirical absorption coefficient for each wavenumber interval considered, such that the expression

$$\mathcal{T} \approx e^{-k_{0\nu}\int_0^{ds}\rho\, ds} \approx 1 - k_{1\nu}\rho\, ds$$

is approximately valid for short path lengths and for the two wavenumber intervals of interest. The coefficient $k_{\Delta\nu}$ was found to vary by a factor of about three over the path lengths considered. Since the generalized absorption coefficient (ℓ_ν) of Elsasser for water vapor, as adopted by Wark et al. (1962) for the same two wavenumber intervals considered here, are within the relevant ranges of $k_{\Delta\nu}$, it was decided to replace $k_{\Delta\nu}$ with these values of ℓ_ν explicitly in order to resolve any ambiguity in the choices of $k_{\Delta\nu}$.

Table 2 gives the values of χ_E , χ_A , ϖ_0 , and g for each of the particle size distributions depicted in Figure 2. The inherent crudeness in calculating the values of g requires that these values be considered only for the purpose of illustration. We shall therefore restrict ourselves for the most part to the wavenumber intervals centered about $\bar{\nu}$ = 889.5 cm^{-1} and $\bar{\nu}$ = 1173.5 cm^{-1}, where water vapor plays a negligible role in the transfer problem. It should be noted that clouds will be most transparent in the infrared window, since elsewhere water vapor, as well as carbon dioxide and perhaps ozone, will tend to increase the effective normal optical thickness [eq. (2.2); cf. also Table 2 and Figure 1].

Table 2. Integrated scattering and absorption parameters characteristic of the particle size distributions and H_2O mixing ratio considered.

$\bar{\nu}$ (cm^{-1})	$D_1(r)$ χ_E (10^{-6} cm^2 per particle)	$D_1(r)$ χ_A (10^{-6} cm^2 per particle)	$D_1(r)$ $\tilde{\omega}_o$	$D_1(r)$ g	$D_2(r)$ χ_E (10^{-6} cm^2 per particle)	$D_2(r)$ χ_A (10^{-6} cm^2 per particle)	$D_2(r)$ $\tilde{\omega}_o$	$D_2(r)$ g
487.5	7.814	4.173	.467	.902	16.57	8.717	.474	.844
889.5	5.197	3.103	.403	1	13.44	7.258	.460	1
1173.5	8.459	1.962	.768	1	16.08	5.596	.652	1
1437.5	8.510	2.451	.712	.391	15.45	6.055	.608	.244

The solid curves in Figures 3a-3d are the phase functions for single scattering integrated over all particle sizes and normalized to $g\tilde{\omega}_o$. Thus

$$p(\cos\Theta) = \frac{\int_0^\infty Q_s \pi r^2 D(r)\, P_r(\cos\Theta)\, dr}{\int_0^\infty Q_s \pi r^2 D(r)\, dr} \tag{3.1}$$

and

$$\int_\omega p(\cos\Theta) \frac{d\omega}{4\pi} = g\tilde{\omega}_o \tag{3.2}$$

where the integration in (3.2) is performed over all solid angles. The dashed curves in the figure are 14-term Legendre polynominal expansions which represent best fits in the sense of least squares. The fits are expressed in the form

$$p(\cos\Theta) = \sum_{\ell=0}^{13} g\tilde{\omega}_\ell' P_\ell(\cos\Theta) , \tag{3.3}$$

where the coefficients $\tilde{\omega}_\ell'$ are constants independent of Θ. These approximations to the relevant phase functions will be the ones used in the remaining numerical solutions. Although the fit for $\bar{\nu}$ = 487.5 cm^{-1} is very good, not enough terms are retained to give completely satisfactory results at larger wave-numbers. More will be said about limitations this will impose on the accuracy of the results in Section 8.

4. Formal Solutions

The specific intensity $I(\tau,\mu)$ refers to the intensity of radiation in the direction μ at a level τ. In order to specify correctly the boundary conditions in a simple manner we shall require that $I(\tau,\mu)$ refer only to the diffuse radiation field which has arisen through one or more scattering and/or emission processes within the cloud itself; thus any radiation from an outside source directly transmitted to the level τ will not be included in the solution. Since (2.1) refers to the total radiation field, it must be modified accordingly.

The intensity of the diffuse radiation field in the direction $+\mu$ at a level τ may be thought to be composed of three components:

1) That component of the intensity which has arisen as a result of the radiation field (from the upper hemisphere) being diffusely reflected by the cloud into the direction μ.
2) That component of the intensity which has arisen as a result of the radiation field (from the lower hemisphere) being diffusely transmitted by the cloud into the direction μ.
3) That component of the intensity which has arisen as a result of thermal emission by the particles within the cloud itself.

We shall suppose that the individual radiation fields do no interfere, and hence may be treated independently.

Consider now a point source removed to infinity in the outward hemisphere.* Let πF_0 be the flux of beam radiation from this point source crossing a unit surface area normal to the beam; further let $(-\mu_0, \phi_0)$ be the direction of propagation of this beam. The azimuth-dependent equation of transfer describing the resultant diffuse radiation field may be written as (cf. Chandrasekhar, 1960; Samuelson, 1964)

$$\mu \frac{dI(\tau,\mu,\phi)}{d\tau} = I(\tau,\mu,\phi)$$

$$- \frac{1}{4\pi} \int_0^{2\pi} \int_{-1}^{+1} p(\mu,\phi;\mu',\phi') \, I(\tau,\mu',\phi') \, d\mu' \, d\phi' \qquad (4.1)$$

$$- \frac{1}{4} F_0 \, e^{-\tau/\mu_0} \, p(\mu,\phi;-\mu_0,\phi_0) \, ,$$

---

* We consider the atmosphere outside the cloud, and the ground, to contribute a radiation field which is made up of a discrete number of point sources. The separate contributions from each point source are added up later in calculating the total contribution.

where $p(\mu,\phi\,;\mu',\phi')$ is the phase function for radiation singly scattered through the angle defined by the direction of incidence (μ',ϕ') and the direction of scattering (μ,ϕ). For a phase function expressible as a finite series expansion of Legendre polynomials [cf. eq. (3.3)] the solution to (4.1) can be formally written as

$$I(\tau,\mu,\phi) = \sum_{n=0}^{N} I^{(n)}(\tau,\mu)\cos n(\phi_0-\phi)\,. \tag{4.2}$$

In particular, the azimuth-independent term in (4.2) obeys the equation

$$\begin{aligned}\mu\,\frac{dI^{(0)}(\tau,\mu)}{d\tau} &= I^{(0)}(\tau,\mu)\\ &\quad-\frac{1}{2}\int_{-1}^{+1} p(\mu,\mu')\,I^{(0)}(\tau,\mu')\,d\mu'\\ &\quad-\frac{1}{4}F_0\,e^{-\tau/\mu_0}\,p(\mu,-\mu_0)\,,\end{aligned} \tag{4.3}$$

where $p(\mu, x)$ refers to the azimuth-independent terms in the expansion in spherical harmonics of $P(\cos\Theta)$ in (3.3); i.e.

$$p(\mu, x) = \sum_{l=0}^{1} \tilde{\omega}_l P_l(\mu) P_l(x) \quad (\tilde{\omega}_1 = g\tilde{\omega}_1') \ . \qquad (4.4)$$

As we shall presently see, the solutions for the remaining terms in (4.2) are of no interest in the context of an axially-symmetric radiation field. We should further note at this time that (2.1) is the correct equation governing the diffuse radiation field arising from thermal emission; i.e., no modification of (2.1) is required in describing the third intensity component cited at the beginning of this section.

The method of discrete ordinates (Chandrasekhar, 1960; Samuelson, 1964) is the method used in this paper to solve (2.1) and (4.3). The continuous radiation field is replaced by 2n linearly independent beams of radiation, n each in the upward and downward directions. This artifice allows the integrals in (2.1) and (4.3) to be replaced by sums, and the resultant system of linear first order differential equations admit closed solutions. The solutions are not analytic in μ, of course, since they are evaluated only at 2n discrete intervals.

The solution to (4.3), in the nth approximation, is of the form

$$I^{(0)}(\tau,\mu_i) = \frac{1}{4}F_0\left\{\sum_{\alpha=1}^{n}\frac{M_\alpha e^{-k_\alpha\tau}}{1+\mu_i k_\alpha}\left[\sum_{l=0}^{N}\varpi_l\,\xi_l(+k_\alpha)P_l(\mu_i)\right]\right.$$

$$+\sum_{\alpha=1}^{n}\frac{M_{-\alpha}e^{+k_\alpha\tau}}{1-\mu_i k_\alpha}\left[\sum_{l=0}^{N}\varpi_l\,\xi_l(-k_\alpha)P_l(\mu_i)\right] \tag{4.5}$$

$$\left.+\frac{\gamma_0 e^{-\tau/\mu_0}}{1+\mu_i/\mu_0}\left[\sum_{l=0}^{N}\varpi_l\,\xi_l\left(\frac{1}{\mu_0}\right)P_l(\mu_i)\right]\right\}$$

$$(i=\pm 1,\ldots,\pm n)\ ,$$

where

$$\left.\begin{aligned}\xi_{l+1} &= -\frac{2l+1-\varpi_l}{k(l+1)}\,\xi_l - \frac{l}{l+1}\,\xi_{l-1}\\ \xi_{-1} &= 0\\ \xi_0 &= 1\end{aligned}\right\} \tag{4.6}$$

$$(l=0,\ldots,N-1)\ ,$$

$$1 = \frac{1}{2}\sum_i a_i\left[\frac{\sum_{\lambda=0}^{N}\varpi_\lambda\,\xi_\lambda(k)P_\lambda(\mu_i)}{1+\mu_i k}\right] \qquad (i=\pm 1,\ldots,\pm n), \tag{4.7}$$

and

$$\gamma_0 = H(\mu_0)\, H(-\mu_0) ,$$

where

$$H(x) = \frac{1}{\mu_1 \cdots \mu_n} \frac{\prod_{i=1}^{n} (x+\mu_i)}{\prod_{\alpha=1}^{n} (1+k_\alpha x)} . \tag{4.8}$$

Once n and N have been chosen, the discrete intervals μ_i $(i = \pm 1, \ldots, \pm n)$ and the Gaussian weights a_i $(i = \pm 1, \ldots, \pm n)$ may be obtained respectively as the zeros of the Legendre polynomial $P_{2n}(\mu)$ and from the formula

$$a_i = \left[\frac{d P_{2n}(\mu)}{d\mu}\right]^{-1}_{\mu=\mu_i} \int_{-1}^{+1} \frac{P_{2n}(\mu)}{\mu-\mu_i}\, d\mu . \tag{4.9}$$

it is always true that

$$\left.\begin{aligned} \mu_i &= -\mu_{-i} \\ a_i &= a_{-i} \end{aligned}\right\} \tag{4.10}$$

for all values of n. For N = 13, n = 7 (the values used in this paper) the values of μ_i and a_i $(i = 1, \ldots, 7)$ are found to be those listed below in Table 3. Equations (4.6) and (4.7) can then be solved interdependently on the electronic computer to obtain the various values of $\xi_\alpha(\mu_i)$ and k_α $(\alpha = \pm 1, \ldots, \pm n)$.

This leaves only the 2n constants of integration $M_{\pm\alpha}$ $(\alpha = 1, \ldots, n)$ to be solved. The requirement that the diffuse radiation field contribute nothing from the upper and lower hemisphere at respectively the top and the bottom of the cloud yields the 2n boundary conditions

$$I^{(0)}(0, -\mu_i) = I^{(0)}(\tau_1, +\mu_i) = 0 \qquad (i = 1, \ldots, n) \;. \tag{4.11}$$

From (4.11) we obtain the 2n equations required to solve for the 2n unknowns, $M_{\pm\alpha}$ $(\alpha = 1, \ldots, n)$, in (4.5). The angular dependence of the outgoing intensity at the top of the cloud is then given by $I^{(0)}(0, +\mu_i)$, and at the bottom of the cloud by $I^{(0)}(\tau_1, -\mu_i)$ (i=1, ..., 7). If the cloud is semi-infinite in extent, all the terms in (4.5) containing $M_{-\alpha}$ $(\alpha = 1, \ldots, n)$ are suppressed, and only the n conditions

$$I^{(0)}(0, -\mu_i) = 0 \qquad (i = 1, \ldots, 7) \tag{4.12}$$

are applied.

Table 3. Gaussian weights and discrete intervals relevant to a 14-Point quadrature formula over the interval (-1, +1)

i	μ_i	a_i
1	0.98628381	0.03511946
2	0.92843488	0.08015809
3	0.82720132	0.12151857
4	0.68729290	0.15720317
5	0.51524864	0.18553840
6	0.31911237	0.20519846
7	0.10805495	0.21526385

Let $I(\tau, \mu')$ be the axially-symmetric intensity of radiation which has arisen as thermal emission in the outward hemisphere and is incident on the cloud at a level τ and in the direction $-\mu'$ (formerly $-\mu_0$). It is convenient to define a scattering function $S(\tau_1 ; \mu, \mu')$ and a transmission function $T(\tau_1 ; \mu, \mu')$ such that the intensity of radiation from the entire upward hemisphere which is diffusely reflected by the cloud into the direction μ is given by

$$I_s(0,\mu) = \frac{1}{2\mu}\int_0^1 S(\tau_1 ; \mu, \mu')\, I_u(0,-\mu')\, d\mu' \qquad (4.13)$$

and the intensity of radiation from the entire lower hemisphere diffusely transmitted through the cloud into the direction μ is given by

$$I_T(0,\mu) = \frac{1}{2\mu}\int_0^1 T(\tau_1;\mu,\mu')\,\mathcal{J}_L(\tau_1,\mu')\,d\mu', \qquad (4.14)$$

where $\tau=\tau_1$ and $\tau=0$ are respectively the normal optical depths at which the cloud bottom and the cloud top are located. In the context of the solution to (4.1) it can be shown (Samuelson, 1964) that S and T obey the relations

$$S(\tau_1;\mu,\mu') = \frac{2\mu}{\pi F_0}\int_0^{2\pi} I_S(0,\mu,\phi)\,d\phi' \qquad (4.15)$$

and

$$T(\tau_1;\mu,\mu') = \frac{2\mu}{\pi F_0}\int_0^{2\pi} I_T(\tau_1,\mu,\phi)\,d\phi', \qquad (4.16)$$

or, by virtue of the axial symmetry exhibited by $\mathcal{J}$ and the form of $I(\tau,\mu,\phi)$ [eq. (4.2)],

$$S(\tau_1;\mu,\mu') = \frac{4\mu}{F_0} I_S^{(0)}(0,\mu) \qquad (4.17)$$

and

$$T(\tau_1; \mu, \mu') = \frac{4\mu}{F_0} I_T^{(o)}(\tau_1, \mu) . \tag{4.18}$$

It should be noted that the sense of direction of $I_T^{(o)}(\tau_1, \mu)$ is reversed in the present context from what it is normally.

Equations (4.13) and (4.14) comprise the solutions to the components of the total outgoing intensity at the cloud top which arise in the first case from the upper, and in the second case from the lower, hemisphere, and are respectively diffusely reflected from and transmitted through the cloud. Upon replacing $B(\tau)$ with the finite power series representation

$$B(\tau) = \sum_{r=0}^{N} b_r \tau^r \tag{4.19}$$

it can be shown (Samuelson, 1964) that the solution to (2.1) for the radiation thermally emitted by the cloud is of the form

$$\begin{aligned} I_E(\tau, \mu_i) = & \sum_{\alpha=1}^{n} \frac{M_\alpha e^{-k_\alpha \tau}}{1+\mu_i k_\alpha} \left[\sum_{\ell=0}^{N} \tilde{\omega}_\ell \xi_\ell(+k_\alpha) P_\ell(\mu_i) \right] \\ & + \sum_{\alpha=1}^{n} \frac{M_{-\alpha} e^{+k_\alpha \tau}}{1-\mu_i k_\alpha} \left[\sum_{\ell=0}^{N} \tilde{\omega}_\ell \xi_\ell(-k_\alpha) P_\ell(\mu_i) \right] \\ & + \sum_{r=0}^{N} \tau^r \left[\sum_{s=r}^{N} c_{r,s} P_{s-r}(\mu_i) \right] \\ & (i = \pm 1, \ldots, \pm n) , \end{aligned} \tag{4.20}$$

where the values of $C_{r,s}$ can be generated by means of the various recursion relations:

$$C_{N,N} = b_N \, , \tag{4.21}$$

$$C_{N-1,N-1} = b_{N-1} \, , \tag{4.22}$$

$$C_{r,N} = \frac{\left[\dfrac{(r+1)(N-r)}{2(N-r)-1}\right]}{\left[1 - \dfrac{\tilde{\omega}_{N-r}}{2(N-r)+1}\right]} C_{r+1,N} \tag{4.23}$$

$$(r = 0, \ldots, N-1) \, ,$$

$$C_{r,N-1} = \frac{\left[\dfrac{(r+1)(N-r-1)}{2(N-r)-3}\right]}{\left[1 - \dfrac{\tilde{\omega}_{N-r-1}}{2(N-r)-1}\right]} C_{r+1,N-1} \tag{4.24}$$

$$(r = 0, \ldots, N-2) \, ,$$

$$C_{r,r} = b_r + \frac{r+1}{3(1-\tilde{\omega}_0)} C_{r+1,r+2} \tag{4.25}$$

$$(r = 0, \ldots, N-2) \, ,$$

and

$$C_{r,s} = \frac{r+1}{\left[1 - \frac{\varpi_{s-r}}{2(s-r)+1}\right]} \left[\frac{s-r+1}{2(s-r)+3} C_{r+1,s+1} + \frac{s-r}{2(s-r)-1} C_{r+1,s} \right] \quad (4.26)$$

$$(s = r+1, \ldots, N-2 \; ; \; r = 0, \ldots, N-3) .$$

The procedure for solving (4.20) is exactly the same as that for (4.5); in particular the boundary conditions (4.11) are incorporated in solving for the 2n constants $M_{\pm\alpha}$ $(\alpha = 1, \ldots, n)$, if the cloud is semi-infinite in extent, conditions (4.12) are used, and the constants $M_{-\alpha}$ $(\alpha = 1, \ldots, n)$ are all suppressed.

5. Cloud Top Radiances

Consider now a plane-parallel model cloudy atmosphere composed of an optically finite cloud imbedded in an otherwise non-scattering atmosphere, bounded on the bottom side by the ground, and on the top side by outer space. Let ($\tau = 0, \tau_1, \tau_2$) be respectively the optical depths at which the cloud top , cloud bottom, and the ground are located. Further let

$$I_D(0,\mu_i) = e^{-\tau_1/\mu_i} \, \mathcal{L}_L(\tau_1, \mu_i) \quad (5.1)$$

be the component of the intensity from the lower hemisphere in the direction μ_i which is directly transmitted through the cloud. The total intensity $I_c(0,\mu_i)$ from the cloud top in the direction μ_i is then the sum of the components directly and diffusely transmitted through, and diffusely reflected and thermally emitted from the cloud. Thus

$$I_c(0,\mu_i) = I_E(0,\mu_i) + I_D(0,\mu_i) + I_T(0,\mu_i) + I_S(0,\mu_i) \quad , \tag{5.2}$$

or, by virtue of (4.13), (4.14), (4.20), and (5.1),

$$\begin{aligned} I_c(0,\mu_i) &= I_E(0,\mu_i) + e^{-\tau_1/\mu_i} \alpha_L(\tau_1,\mu_i) \\ &\quad + \frac{1}{2\mu_i} \int_0^1 T(\tau_1;\mu_i,\mu') \, \alpha_L(\tau_1,\mu') \, d\mu' \\ &\quad + \frac{1}{2\mu_i} \int_0^1 S(\tau_1;\mu_i,\mu') \, \alpha_u(0,-\mu') \, d\mu' \\ &\qquad (i = 1, \ldots, n=7) . \end{aligned} \tag{5.3}$$

The evaluation of the integrals in (5.3) requires a numerical summation. In order to hold the number of terms to a minimum while still maintaining accuracy, the Sykes double-Gauss quadrature formula (King and Florence, 1964) is the one used. Integrals are approximated by

$$\sum_{j=1}^{4} \bar{a}_j \, g(\mu_i, \bar{\mu}_j) \, f(\bar{\mu}_j) = \int_0^1 g(\mu_i, \mu') \, f(\mu') \, d\mu', \qquad (5.1)$$

where the weights $\bar{a}_j$ and the discrete intervals $\bar{\mu}_j$ are listed in Table 4.

Table 4. Weights and discrete intervals relevant to a 4-point quadrature formula over the interval (0, +1)

j	$\bar{\mu}_j$	$\bar{a}_j$
1	0.93056816	0.3478548
2	0.66999052	0.6521452
3	0.33000948	0.6521452
4	0.06943184	0.3478548

The atmosphere chosen to represent typical conditions where California stratus might logically occur is atmosphere #55 listed by Wark, Yamamoto, and Lienesch (1962) and reproduced with minor modifications in Table 5 below. The intensity components [illegible] and $\omega_j(\theta-\bar{\theta})$ $(j = 1, \ldots, 11)$ were obtained from the pressure levels P = 417 mb and P = 950 mb from an IBM 7094 computer program for calculating the infrared radiance of a spherical atmosphere which was furnished to the author by F. Van Cleef of the Meteorological Satellite Laboratory, U. S. Weather Bureau (cf. Wark, Alishouse, and Yamamoto, 1964).

Table 5. Model atmosphere used for calculating intensities incident on cloud boundaries

Pressure (mb)	Temperature (°K)	H_2O (g per kg)	O_3 (cm NTP per mb $\times 10^5$)
1013.0	295	10.7000	000.01
1000.0	292	10.7000	000.01
900.0	290	10.0000	000.40
[illegible]	289	8.3800	000.70
[illegible]	287	8.0000	000.70
[illegible]	285	7.0600	000.90
870.0	283	7.1200	001.20
850.0	292	3.2200	001.50
741.0	285	2.6000	002.10
710.0	280	2.4900	002.60
700.0	285	1.5700	003.00
550.0	267	0.6600	004.90
417.0	259	0.4700	006.00
300.0	250	0.3200	007.50
252.0	242	0.1900	012.50
200.0	219	0.0270	016.50
150.0	209	0.0120	026.50
117.0	203	0.0065	040.00
91.0	203	0.0120	063.00
33.0	216	0.0180	112.50
30.0	218	0.0220	157.50
25.0	228	0.0450	352.50
15.0	233	0.0750	474.00
10.0	236	.1120	525.00
6.0	247	.1120	553.00
4.0	256	.1120	557.50
3.0	263	.1120	523.50
2.0	273	.1120	400.00
1.3	283	.1120	262.50
1.0	283	.1120	175.00
.6	283	.1120	018.00
.4	271	.1120	005.00
.3	262	.1120	003.00
.2	251	.1120	002.00
.1	231	.1120	000.10

The cloud models studied will be restricted to three optical thicknesses (τ_1 = 0.1, 0.5, ∞), two cloud top pressure and temperature levels (P = 417 mb, T = 259 K and P = 950 mb, T = 287 K), and one particle size distribution $D_1(r)$. It will be seen in Section 9 that realistic deviations from isothermal cloud models produce negligible changes in the computed outgoing intensities. Fixing the optical thickness of isothermal clouds renders a description of the angular distribution and net flux of outgoing radiation independent of the actual mass distribution of water in the models [cf. eq. (2.2)]. The two wavenumber intervals considered in detail are the ones (Table 1) centered about $\bar{\nu}$ = 889.5 cm^{-1} and $\bar{\nu}$ = 1173.5 cm^{-1}.

Figures 4a-4f show the computed results for the wavenumber interval centered about $\bar{\nu}$ = 889.5 cm^{-1}. The dotted curve (S) in each separate figure refers to the diffusely reflected component of the intensity [cf. eq. (5.3)],

$$\frac{1}{2\mu}\int_0^1 S(\tau_1;\mu,\mu')\, I_u(0,-\mu')\, d\mu' ,$$

while the lower solid curve (E) refers to the thermally emitted component,

$$I_E(0,\mu) .$$

The reader should be reminded that multiple scattering processes are fully accounted for in the computations of the latter component. The two dashed curves refer to the terms

$$e^{-\tau_1/\mu}\, \mathcal{I}_L(\tau_1, \mu)$$

and

$$\frac{1}{2\mu} \int_0^1 T(\tau_1; \mu, \mu')\, \mathcal{I}_L(\tau_1, \mu')\, d\mu',$$

indicated in the figures by (D) and (T) respectively, the components of the intensity which originate in the lower hemisphere and are respectively directly transmitted and diffusely transmitted through the cloud into the direction μ. These last two components, of course, do not contribute to the net radiation field if the cloud is semi-infinite in extent.

The upper solid curve in each figure is the sum (C) of the four corresponding components, and thus refers to the net radiation field. The dash-dot curve in each case is the standard of comparison (B), i.e., the total intensity which would result at the cloud top if the cloud were of the same optical thickness but composed of nonscattering particles, computed from the expression

$$I_B(0,\mu) = B(T_c) + [\mathcal{I}_L(\tau_1,\mu) - B(T_c)]\, e^{-\tau_1/\mu}, \qquad (5.5)$$

where $B(T_c)$ is the Planck function in intensity units integrated over the relevant wavenumber interval and computed for a cloud temperature T_c.

Perhaps the most remarkable general feature evident in Figures 4a-4f is the lack of an overall marked deviation from greyness for the realistic cloud models, in spite of the fact that the albedo for single scattering is rather high ($\tilde{\omega}_o$ = .403). This is especially true of the low cloud models, where the difference in temperature between the cloud and ground is relatively small.

Figures 5a-5f are the same as Figures 4a-... except that the wavenumber interval is now centered about $\bar{\nu}$ = 1173.5 cm^{-1}, and $\tilde{\omega}_o$ is the higher value of .768. The differences between the upward intensities relevant to the realistic cloud models and those of the corresponding standards of comparison are more marked than the differences illustrated in Figures 4a-4f. This is clearly a result of the higher albedo for single scattering in the wavenumber interval centered around $\bar{\nu}$ = 1173.5 cm^{-1}.

In both wavenumber intervals there is a surplus of radiation (compared with the standards) for optically thin clouds at small zenith angles and a tendency toward a deficit of radiation at large zenith angles. Upon an intercomparison of Figures 4a-4d with Figures 5a-5d for small τ_1, it is noticed that the magnitude of the surplus increases as τ_1, $\tilde{\omega}_0$, and the temperature difference (T_G-T_C) between the ground and the cloud increase; the functional dependence upon μ, however, stays about the same. Again, upon intercomparing Figures 4e-4f and 5e-5f, it is noticed that this surplus becomes a deficit as $\tau_1 \rightarrow \infty$, and the magnitude of this deficit increases as $\tilde{\omega}_0$ increases. It is quite clear, therefore, that the surplus of radiation is primarily due to the radiation diffusely transmitted through the clouds; this radiation is lost from the radiation field in the cases of the standards of comparison.

We must look elsewhere for explanations for the form of the angular distribution of radiation and the deficit of radiation from thick clouds. These explanations are readily obtained from physical considerations discussed in the next section.

C. Physical Considerations

Figures 6 and 7 illustrate the effective emissivities of semi-infinite model clouds for the wavenumber intervals centered respectively about $\bar{\nu}$ = 889.5 cm^{-1} and $\bar{\nu}$ = 1173.5 cm^{-1} as a function of μ. In either figure the upper solid curve (AS) is the effective emissivity $[\epsilon = I_\lambda(0,\mu)/B(T_c)]$ of a cloud having a particle size distribution $D_1(r)$. The lower solid curve (IS) in each figure illustrates the effective emissivity of a cloud composed of particles scattering radiation isotropically with the same respective values of ϖ_0. These latter curves were obtained with the aid of the expression (cf. the Appendix)

$$I_{\Delta\nu}(0,\mu) = (1-\varpi_0)^{\frac{1}{2}} B_{\Delta\nu}(T_c)\, H(\mu) \,, \tag{6.1}$$

where $\Delta\nu$ is the wavenumber interval of interest and $H(\mu)$ is Chandrasekhar's H-function (cf. Chandrasekhar, 1960; Table XI, Chapter V) defined by the nonlinear integral equation

$$H(\mu) = 1 + \frac{1}{2}\varpi_0 \mu H(\mu) \int_0^1 \frac{H(\mu')}{\mu+\mu'} d\mu' \,. \tag{6.2}$$

It is immediately evident from the figures that the forward scattering nature of realistic particles is responsible for the higher values of ϵ, and that higher values of ϖ_0 tend to reduce the magnitude of ϵ in all cases.

Consider now a semi-infinite plane-parallel isothermal cloud composed of partly thermally emitting, partly isotropically scattering particles. All the particles emit radiation at the same rate since they are all at the same temperature. However, the particles at the top of the cloud will scatter radiation at a rate of only about half, say, of the rate at which particles deep within the cloud will scatter radiation, since only about half of the radiation available to the particles deeper in the cloud is available to the particles near the top (the upward hemisphere can contribute nothing at the top). Since the radiation is assumed to be scattered isotropically by each particle, the rate at which radiation is scattered by any particle into any direction in dependent only upon the level τ where the scattering takes place. Hence, the intensity of outgoing radiation at the top of the cloud will be enhanced in the direction $\mu = 1$ over the intensity of radiation in the direction $\mu \sim 0$, because deep layers contribute more to the outgoing intensity in the former case than in the latter for equivalent optical path lengths. Limb darkening is thus explained on physical grounds.

We now overlay the cloud with an optically semi-infinite isothermal slab held at the same temperature as the cloud and allow the radiation field between the two boundaries to achieve a steady state. Conditions at the top of the cloud are now equivalent to conditions within a perfectly insulated isothermal enclosure, and the radiation is "black". The isotropic radiation field from the upward hemisphere incident on the cloud top must therefore contribute to the intensity (in the direction μ) a component of diffusely reflected radiation just sufficient to increase the intensity of radiation thermally emitted by the cloud (in the direction μ) by an amount such that the cloud appears to radiate as a blackbody. The functional relation between this diffusely scattered radiation and μ is thus the "mirror image" of the functional relation between the outgoing thermally emitted radiation at the cloud top and μ, and is illustrated by the upper dashed curves (IS) in Figures 6 and 7.

The lower dashed curves (AS) in the figures refer to the same incident radiation field which is now diffusely reflected from a cloud composed of highly forward scattering particles obeying the size distribution $D_1(r)$. In this case, on the average, each photon is not deviated far from the original direction of incidence even after three of four scattering processes. Due to the rather high finite probability of absorption of each photon-particle interaction, the relative number of photons scattered back into the outward hemisphere is rather small, except for those incident on the cloud top in directions near grazing incidence. Again, because of the extreme forward scattering nature of the cloud particles, even these latter photons must be diffusely reflected primarily into directions corresponding to very small values of μ. Hence, the intensity of radiation diffusely reflected (except perhaps in directions corresponding to $\mu \sim 0$) must be substantially reduced with respect to the intensity of diffusely reflected radiation arising in a medium of isotropically scattering centers. Increasing $\tilde{\omega}_0$ has the effect of raising the curves in general; however, we would not expect a large fraction of the incident radiation to be diffusely reflected (due to the extreme forward scattering nature of the particles) until $\tilde{\omega}_0$ becomes almost unity. It should be noted that in the limit, as the phase function for single scattering becomes completely forward scattering [$p(\cos\Theta) = 0$ for $\Theta \neq 0$] no radiation can be diffusely reflected into the outward hemisphere in <u>any</u> direction ($\tilde{\omega}_0 \neq 1$). The effective emissivity of the cloud must be unity for all μ in this case. We conclude from the foregoing discussion that: (1) increasing $\tilde{\omega}_0$ has the effect of decreasing the overall effective emissivity, (2) the rather high effective emissivity at moderate to large values of μ is due primarily to forward scattering, and (3) the rapid decline in in effective emissivity for small values of μ is due to departures from complete forward scattering.

Analogous arguments may be used to gain insight into the scattering properties of optically thin clouds. In this case we bound both sides of the cloud with isothermal semi-infinite blackbodies. The contribution to the "black" radiation at the cloud top in the direction μ which results from the diffuse reflection of radiation originating in the upper blackbody is in general less than if the cloud were semi-infinitely thick, since some of the radiation from the upper hemisphere passes completely through the cloud in the downward direction and cannot be recovered as outgoing radiation. An isothermal composite made up of an optically finite cloud overlying a semi-infinite perfect absorber and emitter is thus seen to have an effective emissivity somewhere between those of a semi-infinite cloud and a perfect blackbody.

It is quite clear, therefore, that the surplus of outgoing radiation at the top of the optically finite cloud models depicted in Figures 4a-4d and 5a-5d, compared with the relevant perfectly absorbing and emitting standards, is due to the temperature difference between the (warmer) ground and the cloud models. The difference is accentuated by the forward scattering nature of the cloud particles; i.e., the radiation incident on each cloud bottom, which is scattered, is primarily diffusely transmitted through the cloud in the forward direction, and very little is diffusely reflected back into the lower hemisphere.

Upon referring to Table 2 we note that the effective cross sections ($\frac{1}{g} N_0 \chi_E$) of a unit volume mass element is smaller at $\bar{\nu}$ = [illegible].5 cm^{-1} and 1173.5 cm^{-1} than at $\bar{\nu}$ = 487.5 cm^{-1} and 1437.5 cm^{-1} for the particle size distribution $D_1(r)$, and the effective albedos for single scattering, $g\tilde{\omega}_0$, are larger. The smaller values of $\frac{1}{g} N_0 \chi_E$ will have the effect of decreasing the normal optical thickness τ_1 of a given cloud, and the larger values of $g\tilde{\omega}_0$ will have the effect of increasing the net flow of outgoing radiation through the cloud. Both considerations would lead us to expect a surplus of net outgoing radiation in the window region of the infrared spectrum compared to that which would be calculated under the assumption of "grey" clouds, where the ground is considerably warmer than the cloud. We should, of course, expect a deficit if the ground is cooler than the cloud, or if the cloud is very thick.

7. The Net Flux and Angular Distribution of Radiation From the Top of the Atmosphere

It is evident that the outgoing intensity $I(0,\mu_i)$ at the top of a cloud atmosphere is given by the relation

$$I(0,\mu_i) = \mathcal{L}(\mu_i) + T(\mu_i)\, I_c(0,\mu_i) \qquad (7.1)$$

$$(i = 1, \ldots, n = 7)$$

where $I_c(0,\mu_i)$ is the total intensity in the direction μ_i at the top of the cloud as previously considered, $T(\mu_i)$ is the transmission function through the overlying atmosphere in the direction μ_i for the wavenumber interval of interest, and $J(\mu_i)$ is the outgoing intensity at the top of the overlying atmosphere due to thermal emission from that stratum. Both $J(\mu_i)$ and $T(\mu_i)$ were calculated with the program furnished by F. Van Cleef which was mentioned previously.

Figures 8a-8b and 9a-9b illustrate the limb darkening at the top of the atmosphere for each of the previously considered cloudy atmosphere models, and Table 6 gives the net outgoing flux πF, derived from the expression (cf. Table 3)

$$F = 2 \sum_{j=1}^{7} a_j \mu_j I(0,\mu_j) \quad , \tag{7.2}$$

for each of these models. All values in the table are relative to the fluxes for clear sky conditions, and these fluxes have been normalized to unity for each wavenumber interval.

Table 6. Relative outgoing fluxes at the top of the atmosphere normalized to the clear sky flux

$\bar{\nu}$ (cm^{-1})	889.5						1173.5					
P(mb)	950			417			950			417		
τ_1	0.1	0.5	∞	0.1	0.5	∞	0.1	0.5	∞	0.1	0.5	∞
F	.992	.969	.920	.948	.826	.573	.994	.967	.876	.963	.867	.454
F_B	.989	.960	.924	.931	.769	.579	.986	.949	.902	.917	.721	.490

It is immediately obvious from the figures that thin clouds considerably cooler than the effective radiating surface below them are most effective in producing strong limb darkening. In comparison with the relevant standards, limb darkening in realistic cases is somewhat less at moderate values of μ and greater at very small values of μ. The low cloud cases studied show limb darkening comparable in magnitude to those of clear sky conditions, while the high cloud cases show much stronger darkening.

Atmospheres containing optically thick clouds still show limb darkening, but to a much smaller degree. Since we have seen qualitatively that the sharp increase in darkening at small values of μ is a function of the degree of forward scattering by individual particles, it should be possible in principle to obtain an idea of the effective particle sizes near the tops of thick cloud systems through an analysis of limb darkening curves obtained by airborne radiometers. Measurements near grazing angles would be most critical.

Table 6 shows, in effect, the relative surplus (compared with the relevant standards, subscripted with B) of the net outgoing flux at the top of the atmosphere in which are imbedded clouds of small optical thickness, and the relative deficit of flux where the optical thicknesses of the imbedded clouds are infinite. It is seen that the respective surpluses and deficits are most marked for $\bar{\nu} = 1173.5\ cm^{-1}$. In particular, the outgoing net flux at the top of the atmosphere containing a semi-infinite cloud (the top of which is located at P = 417 mb) is only .927 of the outgoing net flux computed on the basis of assuming the cloud to be black. Conversely, the corresponding flux ratio at the top of the atmosphere containing a cloud of normal optical thickness $\tau_1 = 0.1$ at the same level is 1.050. For a cloud of normal optical thickness $\tau_1 = 0.5$ this ratio becomes 1.203. Other ratios derivable from the table, while not so dramatic, follow the same pattern.

8. Computational Errors

It is desirable to retain as many terms in (3.3) as possible for obvious reasons (cf. Figures 3a-3d). There will, however, be a point beyond which N cannot be increased without destroying acceptable accuracy in the solutions to (4.5) and (4.20) as a result of rounding errors in the computer program. One critical area of computation centers around the simultaneous solutions of (4.6) and (4.7) for the values of k_α $(\alpha = \pm 1, \dots, \pm n)$ and $\xi_l(k_\alpha)$ $(l = 0, \dots, N)$. A check on the accuracy of the various values of $\xi_l(k_\alpha)$ was obtained from the expression

$$\xi_\ell(k_\alpha) - \frac{1}{2} \sum_i a_i P_\ell(\mu_i) \left[\frac{\sum_{\lambda=0}^{N} \varpi_\lambda \xi_\lambda(k_\alpha) P_\lambda(\mu_i)}{1 + \mu_i k_\alpha} \right] = 0 \qquad (8.1)$$

$$(i = \pm 1, \ldots, \pm n \; ; \; \ell = 0, \ldots, N)$$

for all values of k_α $(\alpha = \pm 1, \ldots, \pm n)$. It is cl ar from (4.6) that the greatest trouble will occur for $|k| < 1$ and $\ell = N$; this was in fact verified numerically from (8.1). The criterium finally arrived at by trial and error was that the magnitude of the left-hand side of (8.1) should always be less than 10^{-4} in order to guarantee a comparable accuracy in (4.5) and (4.20) for $\tau_1 \leq 1$. This required, under the present computational scheme, a limiting of the values of N and n to those indicated in this paper. It should be noted that increasing the magnitude of τ_1 beyond unity will correspondingly decrease the accuracy of (4.5) and (4.20), since terms of the form $e^{\pm k_\alpha \tau_1}$ occur in pairs in these equations, and the matrix solutions for the 2n constants $M_{\pm\alpha}$ $(\alpha = 1, \ldots, n)$ from the 2n boundary conditions [cf. eq. (4.11)] are critically dependent upon the difference in magnitudes of the various terms in the systems of equations to be solved. In order to be on the safe side it was [illegible]d to restrict the study of optically finite cloud models to those of normal optical thickness $\tau_1 \leq 0.5$. As we shall see in Section 9, this does not unduly restrict the scope of the study.

Another important source of error centers around replacing the various integrals encountered with Gaussian sums. Since single scattering contributes significantly to the diffuse radiation field for the values of $\tilde{\omega}_0$ used, the diffuse reflection and transmission functions S and T tend to maintain the oscillatory nature of the phase function for single scattering (cf. Figures 3a-3d), and are thus not amenable to reproduction through the use of polynomials of low degree. Hence, the use of a quadrature formula of low degree [eq. (5.4)] for evaluating the integrals in (5.3) will be source of considerable error. The maximum errors were found to be involved in calculating the integrals of the scattering function illustrated in Figure 7, and the integrals of the transmission functions illustrated in Figures 5c-5d, as indicated by the crosses in each figure. It is quite clear that the actual computations will not yield acceptable accuracy as they stand.

However, it is extremely desirable to limit the number of explicit calculations of $\mathcal{J}_L(\tau_1, \bar{\mu}_i)$ and $\mathcal{J}_u(0, -\bar{\mu}_i)$ in (5.3) to a minimum, since each of these computations is in itself quite involved. The artifice of correcting the computations by means of physical considerations brought out in the last section appear to yield quite satisfactory results. The format for making and applying these corrections is given below.

1. The computed values of $I_E(0, \mu_i)$ are assumed to be correct as they stand. It should be noted that the oscillatory nature of the phase function for single scattering is not maintained in the thermal component of the intensity, due to the diffuse nature of the radiation source. The correctness of the quadrature formula incorporated implicitly in the solutions of (4.20), and thus also in (4.5) and (7.1), would appear to be established in view of the essentially identical results obtained for $I_E(0, \mu_i)$ $(i = 1, \ldots, n)$ for several test computations involving different values of N and n. In particular, the values of N tested were N = 7, 9, 11, 13, and 15, and the corresponding values of n were n = 4, 5, 6, 7, and 8; only for N = 7 and n = 4 did the smooth curve fitted through the computed values differ from the smooth curves fitted through the values for other cases.

2. The only additional component to the outgoing radiation field at the top of semi-infinite clouds is the one due to diffuse reflection. The relevant integral (4.13) was evaluated for conditions equivalent to those inside a perfectly insulated isothermal enclosure; i.e., $\mathcal{I}_u(0,-\bar{\mu}_j)$ was set equal to $B(T_c)$ for all $\bar{\mu}_j$ $(j = 1, \ldots, 4)$, and $I_s(0,\mu_i)$ evaluated for all μ_i $(i = 1, \ldots, 7)$. Each computed value of $I_s(0,\mu_i)$ was then corrected by the relative amount required to agree with the corresponding mirror image of $I_E(0,\mu_i)$. These relative corrections were then applied to the integrals computed which describe the intensity of radiation arising from the anisotropic radiation in the upward hemisphere that is diffusely reflected into the relevant direction μ_i. In all cases considered the <u>absolute</u> corrections required were very small, primarily because the diffusely reflected component itself is quite small (cf. Figures 4e-4f and 5e-5f).

3. Corrections for the diffusely transmitted components through clouds of small optical thickness were computed in essentially the same way. In this way all the values of $\mathcal{I}_u(0,-\bar{\mu}_j)$ and $\mathcal{I}_L(\tau_1,\bar{\mu}_j)$ in (4.13) and (4.14) were set equal to $B(T_c)$.

The computed values of $I_E(0,\mu_i)$, $I_D(0,\mu_i)$, and $I_S(0,\mu_i)$ i (5.2) were then added and the sum subtracted from $B(T_c)$. The calculated values of $I_T(0,\mu_i)$ were then corrected to these values, and the relative corrections thus obtained applied to the relevant diffuse transmission integral in (5.3) describing the radiation diffusely transmitted through the cloud arising from the anisotropic radiation field of the lower hemisphere. The errors introduced by assuming $I_S(0,\mu_i)$ to be exact should be negligible by virtue of the smallness of $I_S(0,\mu_i)$ itself. The corrected points, illustrated for example in Figure 4c-4d and 5c-5d by the open circles, were gratifyingly close to a smooth curve fitted through the points in all cases.

The essential assumption required in making these correction is that the <u>form</u> of the integrals thus corrected does not depend critically on the nature of the incident radiation field. Since only the integrals over the transmission functions would appear to be a cause of much concern in the cases studied, and since the radiation field in the lower hemisphere is essentially isotropic in all cases, the corrections applied may confidently be expected to effect a quite accurate solution. Inaccuracies of up to one percent may still be inherent in the solutions.

Tests of other possible sources of error in the computations were made wherever required, and all errors thus found were determined to be negligible -- on the order of 10^{-7} or less.

9. Effects of an Arbitrary Temperature Gradient and Normal Optical Thickness

The cloud models adopted in this study have been isothermal. Table 7 shows the effect on $I_E(0,\mu_i)$ which is obtained by assuming a moist adiabatic lapse rate of 5K km^{-1} through a semi-infinite cloud. The particle densities assumed are $N_o = 100$ particles cm^{-3} for a cloud top temperature $T_c = 259K$, and $N_o = 300$ particles cm^{-3} for $T_c = 287K$. It is seen that the effect of a realistic temperature gradient through the cloud is quite small in comparison with a zero gradient, and hence may in general be quite safely neglected.

Table 7. Effect of a temperature gradient dT/dz on the angular distribution of outgoing radiation at the top of a semi-infinite cloud

Discrete interval i	$\bar{\nu} = 889.5\ cm^{-1}$			$\bar{\nu} = 1173.5\ cm^{-1}$		
	$-\frac{dT}{dz} = 0$	$-\frac{dT}{dz} = 5K\ km^{-1}$		$-\frac{dT}{dz} = 0$	$-\frac{dT}{dz} = 5K\ km^{-1}$	
	$I_{\Delta\nu}/F$	$I_{\Delta\nu}/F$		$I_{\Delta\nu}/F$	$I_{\Delta\nu}/F$	
		$T_c = 287K$, $N_o = 300$ (particles cm^{-3})	$T_c = 259K$, $N_o = 100$ (particles cm^{-3})		$T_c = 287K$, $N_o = 300$ (particles cm^{-3})	$T_c = 259K$, $N_o = 100$ (particles cm^{-3})
1	1.00605	1.00637	1.00725	1.03687	1.03724	1.03825
2	1.00549	1.00574	1.00646	1.03386	1.03416	1.03497
3	1.00476	1.00491	1.00535	1.02836	1.02853	1.02900
4	1.00225	1.00227	1.00231	1.01561	1.01562	1.01563
5	.99778	.99763	.99721	.99209	.99190	.99139
6	.98178	.98144	.98051	.93356	.93319	.93218
7	.91843	.91793	.91657	.77678	.77632	.77507

The effect of a temperature gradient on an optically thin cloud would be expected to be much less. An idea of the relation among T, z, and τ_1 calculated with the aid of equation (2.2) and Table 2, is illustrated in Figure 10 for the particle density N_o = 100 particles cm^{-3} previously cited. This figure is also useful for obtaining an estimate of the normal optical thicknesses to be associated with the geometrical thicknesses of various clouds.

Consider now a perfectly absorbing and emitting (nonscattering cloud having a temperature T_c and overlying an isotropically emitting ground radiating at twice the rate characteristic of a semi-infinite blackbody of temperature T_c. Figure 11 is a parametric representation in terms of τ_1 of the angular distribution of radiation at the top of the cloud, computed from expression (5.5), where $\mathcal{J}_L(\tau_1, \mu_i) = 2B(T_c)$. It would appear from the figure that the values of τ_1 considered in this study are quite representative of the extreme cases of interest, and that judicious interpolations for the scattering properties of clouds having other optical thicknesses are quite feasible.

10. Conclusions

Some general summarizing statements may now be made regarding the infrared radiative characteristics of plane-parallel clouds. If a cloud is much cooler than the effective radiating level below the cloud, it follows that:

1. A considerable surplus flux of outgoing radiation in the window region of the infrared spectrum would be expected for thin clouds compared to what would be calculated if scattering were not taken into account. In general we would also expect clouds to be considerably poorer absorbers in the window region than over the infrared spectrum as a whole. This is due to the fact that clouds are both optically thinner and better scatterers in the window. We would furthermore expect the scattered radiation to be predominantly diffusely transmitted through the cloud rather than diffusely reflected by the cloud because of the forward scattering nature of the individual particles making up the cloud. This in general would lead to a "surplus" of outgoing radiation in the window.

2. A deficit of outgoing radiation would be expected in the window from optically thick clouds (i.e. $\epsilon < 1$), and from thin clouds warmer than the effective radiating layer below them. This deficit, however, is minimized considerably by the forward scattering nature of individual particles.

3. Limb darkening in general is evident in all cases to a greater extent than would be anticipated by treating clouds as infinitely thick isothermal blackbodies. Limb darkening is considerable at very large zenith angles, and even more greatly enhanced in general if the clouds are thin and much cooler than th effective radiating layer below them.

4. A realistic temperature gradient in clouds is of almost n importance. It should be noted, however, that we have considered only single layers; multiple decks of clouds have not been treate

In practice the concept of plane-parallel clouds is quite unrealistic except in special circumstances. Clouds are generall quite "corrugated" at the top. These corrugations may take the form of mounds, billows, waves, and many other shapes. Furthermor clouds do not have infinite horizontal extent, and because they ar often quite thick geometrically there is a projection factor to be taken into account. This projection factor is necessary to proper account for the apparent greater cloud cover at large zenith angl than at small angles. Any general statistical analysis of the radiative characteristics of the Earth's cloudy atmosphere must therefore be modified in accordance with these views.

Nevertheless the preceding calculations are of considerable ai in obtaining a qualitative picture of what one would expect to fin from statistical studies. In particular, if clouds are primarily cumulus in type, one would expect ϵ to be slightly less than unity and almost independent of zenith angle. This follows from considering cumulus clouds to be optically thick and somewhat hermispherical in shape. Any zenith angle would correspond roughly to normal viewing incidence because of the hemispherical shape of the cloud. Hence, ϵ (cf. Figures 6-7) would be rather high regardless of the value of μ.

If thin clouds over very warm surfaces are present, a surpl flux of radiation would still be expected in the infrared window for the reasons previously cited, since very thin clouds would be expected to behave as though they were stratified. If the effective radiating level were cooler than the cloud a flux deficit could be expected in the window.

Multiple cloud decks have not been treated because of the considerably greater complexity in the theory resulting from the scattering of radiation back and forth between layers. In reality, of course, multiple cloud systems are not uncommon. If the particle size distribution remains constant from layer to layer, and the effects of the gaseous atmosphere between layers is ignored, then, in the first approximation, the several decks may be regarded as one continuous cloud. Because this "single" cloud is extended over a large vertical distance, the temperature becomes a strong function of optical depth. Thus

$B(\tau)$ is no longer sensibly constant over the entire range of τ. The effect of increasing $B(\tau)$ with increasing τ would be that of causing stronger limb darkening than calculated previously in this paper (cf. Table 7).

It would be very useful to extend the investigation to include more intervals of the infrared spectrum, as well as to expand the investigation to include more particle size distributions and values of the normal optical thickness τ_1. It should further be noted that an extension to ice clouds would be of paramount interest, since absorption by ice in the infrared window is much lower in general than absorption by water (Kislovskii, 1963). Consequently $\tilde{\omega}_0$ in general should be much higher for ice particles and deviations from unit emissivity possibly quite large for clouds composed of such particles. Since these particles (crystals) are in general not spherical, the Mie theory, strictly speaking, is inapplicable in describing single scattering; it follows that a discussion of effective emissivities of ice clouds is beyond the scope of this paper.

Acknowledgements. There remains only the pleasant task of expressing my thanks to Mr. F. Van Cleef for furnishing and discussing in some detail the program used to compute

the necessary intensities and transmission functions for the clear atmosphere, to Mr. T. Michels for modifying and furnishing the program used to compute the relevant Mie scattering parameters, and to Mr. J. D. Barksdale for writing the program used to solve the basic equation of transfer. All computations were performed on the IBM 7094 digital computer.

APPENDIX

Solution to $I_E(0,\mu)$ in the Context of Isotropically Scattering Particles

The law of diffuse reflection from a semi-infinite medium in the context of isotropically scattering particles is given by (Chandrasekhar, 1960)

$$I_S^{(0)}(0,\mu) = \frac{1}{4}\varpi_0 F_0 \frac{\mu_0}{\mu+\mu_0} H(\mu) H(\mu_0) \qquad \text{(A.1)}$$

where πF_0 is the incident flux of beam radiation from a point source which crosses (in the direction $-\mu_0$) a unit area normal to the beam, and where $H(\mu)$ is defined by the nonlinear integral equation

$$H(\mu) = 1 + \frac{1}{2}\varpi_0 \mu H(\mu) \int_0^1 \frac{H(\mu')}{\mu+\mu'} d\mu' \qquad \text{(A.2)}$$

By virtue of (4.13) and (4.17) the intensity of radiation from all directions in the upward hemisphere which is diffusely reflected into the direction μ is

$$\mathring{I}_S(0,\mu) = 2\int_0^1 \frac{1}{F_0} I_S^{(0)}(0,\mu)\, \delta_u(0,-\mu_0)\, d\mu_0\,, \qquad \text{(A.3)}$$

or, from (A.1),

$$I_s(0,\mu) = \frac{1}{2}\varpi_0 H(\mu) \int_0^1 \frac{\mu_0 H(\mu_0)}{\mu+\mu_0} \mathcal{J}_u(0,-\mu_0)\, d\mu_0 \, . \tag{A.4}$$

Now let

$$\mathcal{J}_u(0,-\mu_0) = B_{\Delta\nu}(T_c) \tag{A.5}$$

for all μ_0 , where $B_{\Delta\nu}(T_c)$ is the Planck function over the interval $\Delta\nu$ characteristic of the cloud temperature T_c. This artifice renders conditions at the cloud top equivalent to conditions within a perfectly insulated isothermal cavity, and (A.4) becomes

$$I_s(0,\mu) = \frac{1}{2}\varpi_0 B_{\Delta\nu}(T_c) H(\mu) \int_0^1 \frac{\mu_0 H(\mu_0)}{\mu+\mu_0}\, d\mu_0 \, . \tag{A.6}$$

Upon using (A.2) and replacing $\frac{\mu_0}{\mu+\mu_0}$ in the integrand of (A.6) with

$$\frac{\mu_0}{\mu+\mu_0} = 1 - \frac{\mu}{\mu+\mu_0} \; , \tag{A.7}$$

we obtain

$$I_s(0,\mu) = B_{\Delta\nu}(T_c)\left[\frac{1}{2}\varpi_0 H(\mu)\int_0^1 H(\mu_0)\, d\mu_0 + 1 - H(\mu)\right] . \tag{A.8}$$

Again, upon multiplying (A.2) by $\frac{1}{2}\varpi_0$ and integrating over the range of μ, we obtain

$$\frac{1}{2}\varpi_0 \int_0^1 H(\mu)\,d\mu = \frac{1}{2}\varpi_0 + \frac{1}{4}\varpi_0^2 \int_0^1\int_0^1 \frac{\mu}{\mu+\mu_0} H(\mu)H(\mu_0)\,d\mu_0\,d\mu , \qquad \text{(A.9)}$$

or, upon interchanging μ and μ_0 and adding,

$$2\left[\frac{1}{2}\varpi_0 \int_0^1 H(\mu)\,d\mu\right] = \varpi_0 + \left[\frac{1}{2}\varpi_0 \int_0^1 H(\mu)\,d\mu\right]^2 . \qquad \text{(A.10)}$$

Solving the quadratic in (A.10) for the intergral gives us

$$\frac{1}{2}\varpi_0 \int_0^1 H(\mu)\,d\mu = 1 \pm (1-\varpi_0)^{\frac{1}{2}} . \qquad \text{(A.11)}$$

Since $H(\mu)$ converges uniformly to unity as ϖ_0 uniformly approaches zero [cf. eq. (A.2)], we must choose the minus sign in (A.11) in order to preserve the identity for all ϖ_0 .

By virtue of (A.11) we obtain for (A.8) the result

$$I_s(0,\mu) = B_{\Delta\nu}(T_c)\left[1 - (1-\varpi_0)^{\frac{1}{2}} H(\mu)\right] . \qquad \text{(A.12)}$$

We have solved the problem in the context of conditions within an isothermal cavity, where the cloud top is one of the perfectly insulated bounding surfaces. It follows from Kirchhoff's law that the thermally emitted component of radiation from the cloud is given by

$$I_E(0,\mu) = B_{\Delta\nu}(T_c) - I_s(0,\mu) , \tag{A.13}$$

or, from (A.12),

$$I_E(0,\mu) = (1-\varpi_0)^{\frac{1}{2}} B_{\Delta\nu}(T_c)\, H(\mu) , \tag{A.14}$$

and the desired result is established.

REFERENCES

Chandrasekhar, S., 1946 : On the Radiative Equilibrium of a Stellar Atmosphere. XII. *Astrophys. J.*, *104*, 191-202.

________________, 1960 : *Radiative Transfer*. New York, Dover Publications, Inc., 393 pp.

King, Jean I. F., and E. T. Florence, 1964 : Moment Method for Solution of the Schwarzschild-Milne Integral Equation. *Astrophys. J.*, *139*, 397-403.

Kislovskii, L. D., 1959 : Optical Characteristics of Water and Ice in the Infrared and Radiowave Regions of the Spectrum. *Opt. i Spec.*, *7*, 201-206.

Neiburger, M., 1949 : Reflection, Absorption, and Transmission of Insolation by Stratus Cloud. *J. Met.*, *6*, 98-104.

Penndorf, R. B., 1963 : Research on Aerosol Scattering in the Infrared. Final Report AFCRL-63-668. Published as Research and Advanced Development Division AVCO Corporation Technical Report, RAD-TR-63-26, 231 pp. Available at cost through the U. S. Department of Commerce, Office of Technical Services, Washington , D. C. 20235.

Samuelson, R. E., 1965 : Radiative Transfer in a Cloudy Atmosphere. NASA Technical Report, R-215. Available at cost through the U. S. Department of Commerce, Office of Technical Services, Washington , D. C. 20235.

REFERENCES (Continued)

Wark, D. Q., J. Alishouse, and G. Yamamoto, 1964 : Variation of the Infrared Spectral Radiance near the Limb of the Earth. Appl. Opt., 3, 221-227.

________________________, G. Yamamoto, and J. Lienesch, 1962 : Infrared Flux and Surface Temperature Determinations from TIROS Radiometer Measurements. U. S. Weather Bureau, Meteorological Satellite Laboratory Report No. 10, 84 pp. Available at cost through the U. S. Department of Commerce, Office of Technical Services, Washington, D. C. 20235, N-63 - 11881.

FIGURE LEGENDS

Figure 1. Complex index of refraction of water ($\tilde{n} = n - ik$) as a function of the wavenumber ν in inverse centimeters.

Figure 2. Particle size distributions (modified from Neuburger) representative of California stratus and the Mie efficiency factors Q_E and Q_A as a function of $\bar{\nu}$ and particle diameter d. The computed points for Q_E and Q_A are indicated respectively by circles and triangles.

Figure 3. Phase functions for a single scattering $p(\cos\theta)$ in arbitrary units as a function of the scattering angle

Figure 4. Contribution to the total intensity (C) at the cloud top from the components respectively diffusely reflected (S), thermally emitted (E), directly transmitted (D), and diffusely transmitted (T) for the wavenumber interval centered about $\bar{\nu} = 889.5\ cm^{-1}$. All intensities, including the standard of comparison (B), are on the same (but arbitrary) scale.

Figure 5. Same as Figure 4 for the wavenumber interval centered about $\bar{\nu} = 1173.5\ cm^{-1}$.

Figure 6. Effective emissivities (solid curves) and diffuse reflectances (dotted curves) of semi-infinite clouds for $\tilde{\omega}_0 = .403$. The curves labeled (AS) and (IS) refer to anisotropic and isotropic scattering respectively. All curves are normalized to unity.

Figure 7. Same as Figure 6 for $\tilde{\omega}_0 = .768$.

Figure 8. Limb darkening at the top of the atmosphere in the wavenumber interval centered about $\bar{\nu} = 889.5\ \mathrm{cm}^{-1}$. The normal optical thickness of each cloud model imbedded in the atmosphere is indicated by the relevant value of τ_1, and each cloud is located at a height characteristic of the indicated pressure P.

Figure 9. Same as Figure 8 for the wavenumber interval centered about $\bar{\nu} = 1173.5\ \mathrm{cm}^{-1}$.

Figure 10. Relation among the temperature difference ΔT, geometrical depth ΔZ, and normal optical depth τ for a particle density $N_0 = 100$ particles cm^{-3} and a cloud top temperature $T_c = 259K$.

Figure 11. Limb darkening for isothermal nonscattering clouds of temperature T_c as a function of the parameter τ_1. The ground is assumed to be a blackbody of temperature T_G radiating at a rate $B(T_G) = 2B(T_c)$.

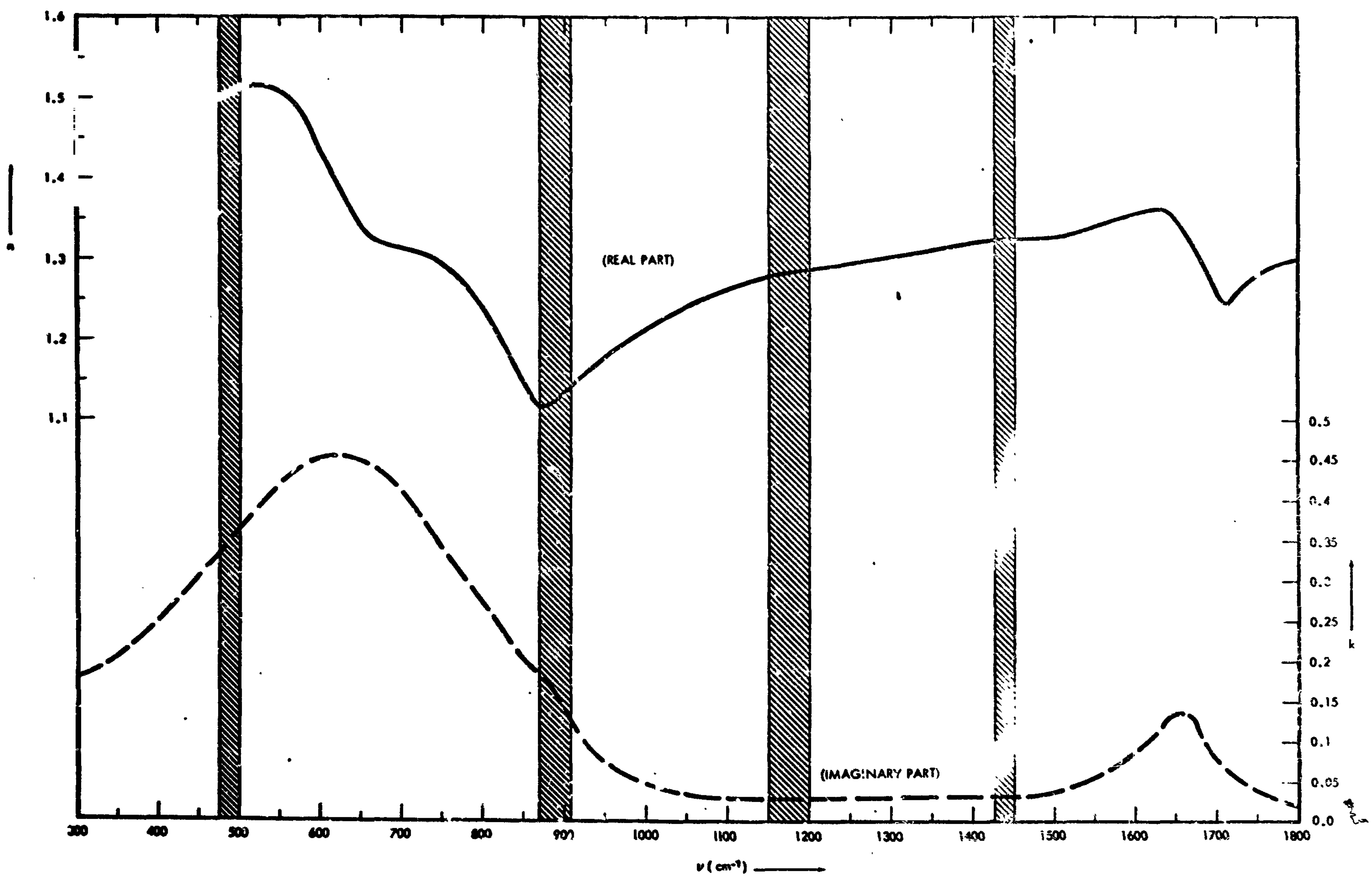

1.6
1.5
1.4
1.3
1.2
1.1
n
(REAL PART)
(IMAGINARY PART)
0.5
0.45
0.35
0.25
0.2
0.15
0.1
0.05
0.0
k
300
400
500
600
700
800
1000
1100
1200
1300
1400
1500
1600
1800
ν (cm⁻¹)

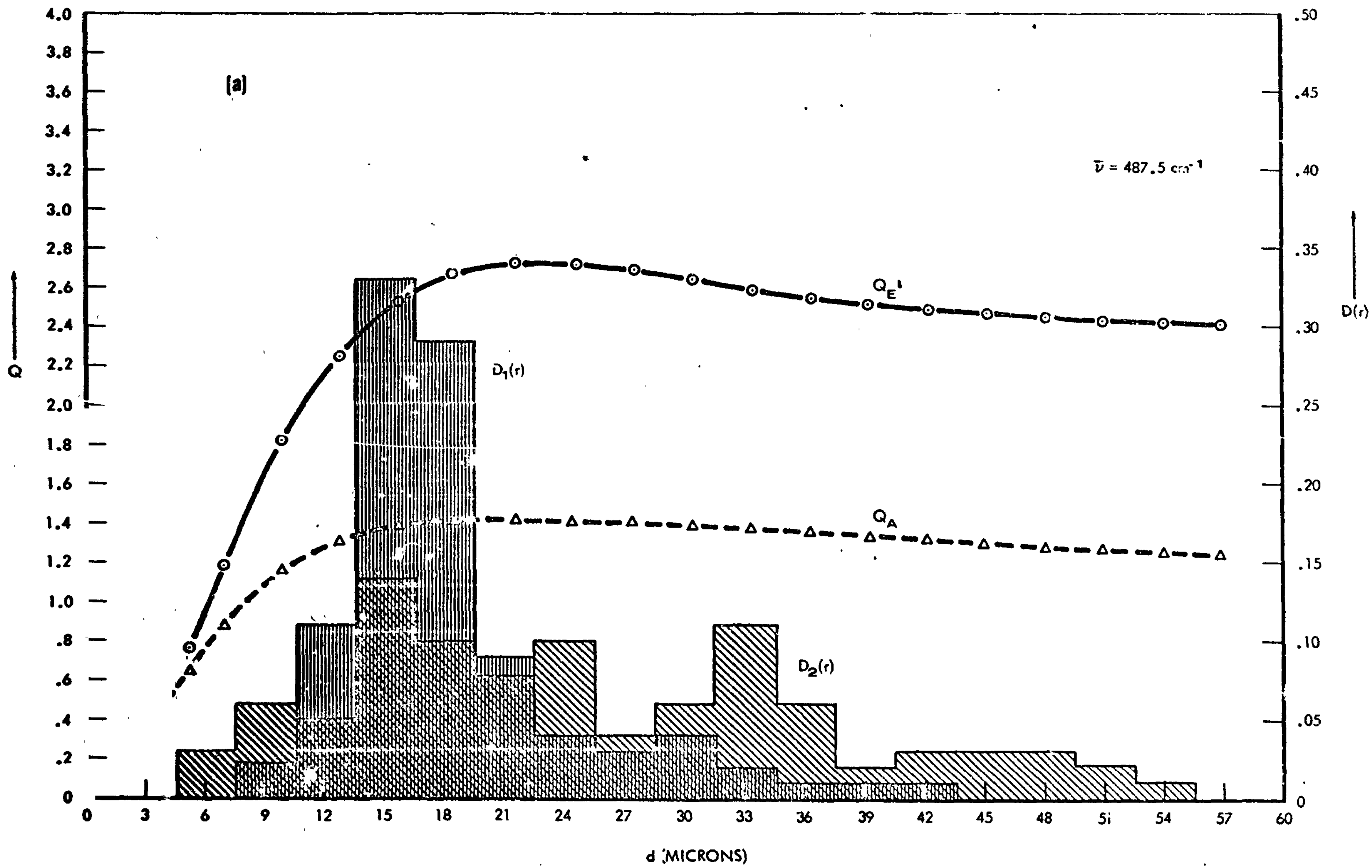

(a)
$\bar{\nu}$ = 487.5 cm⁻¹
Q_E'
Q_A
$D_1(r)$
$D_2(r)$
Q
D(r)
d (MICRONS)

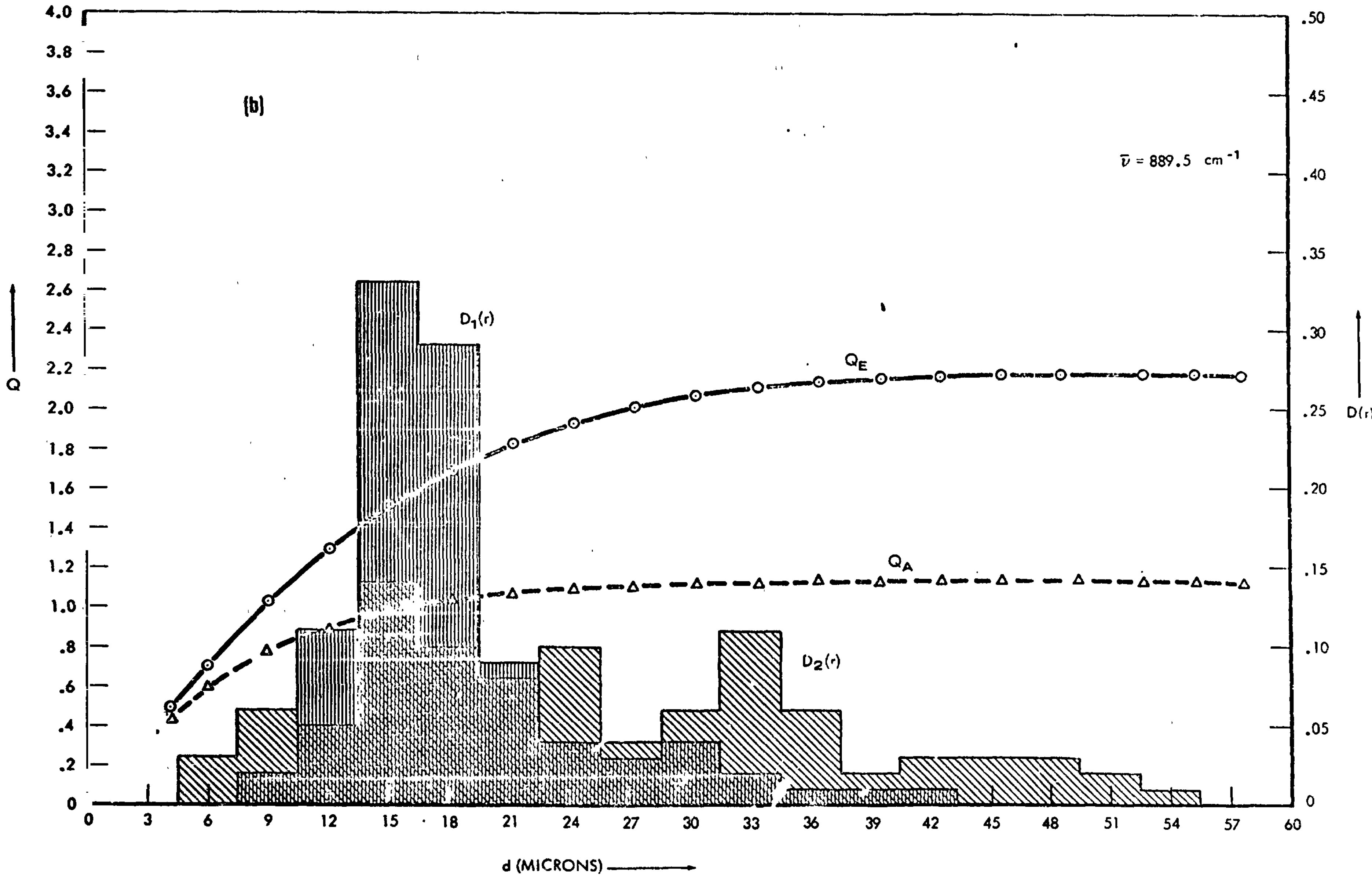

F...

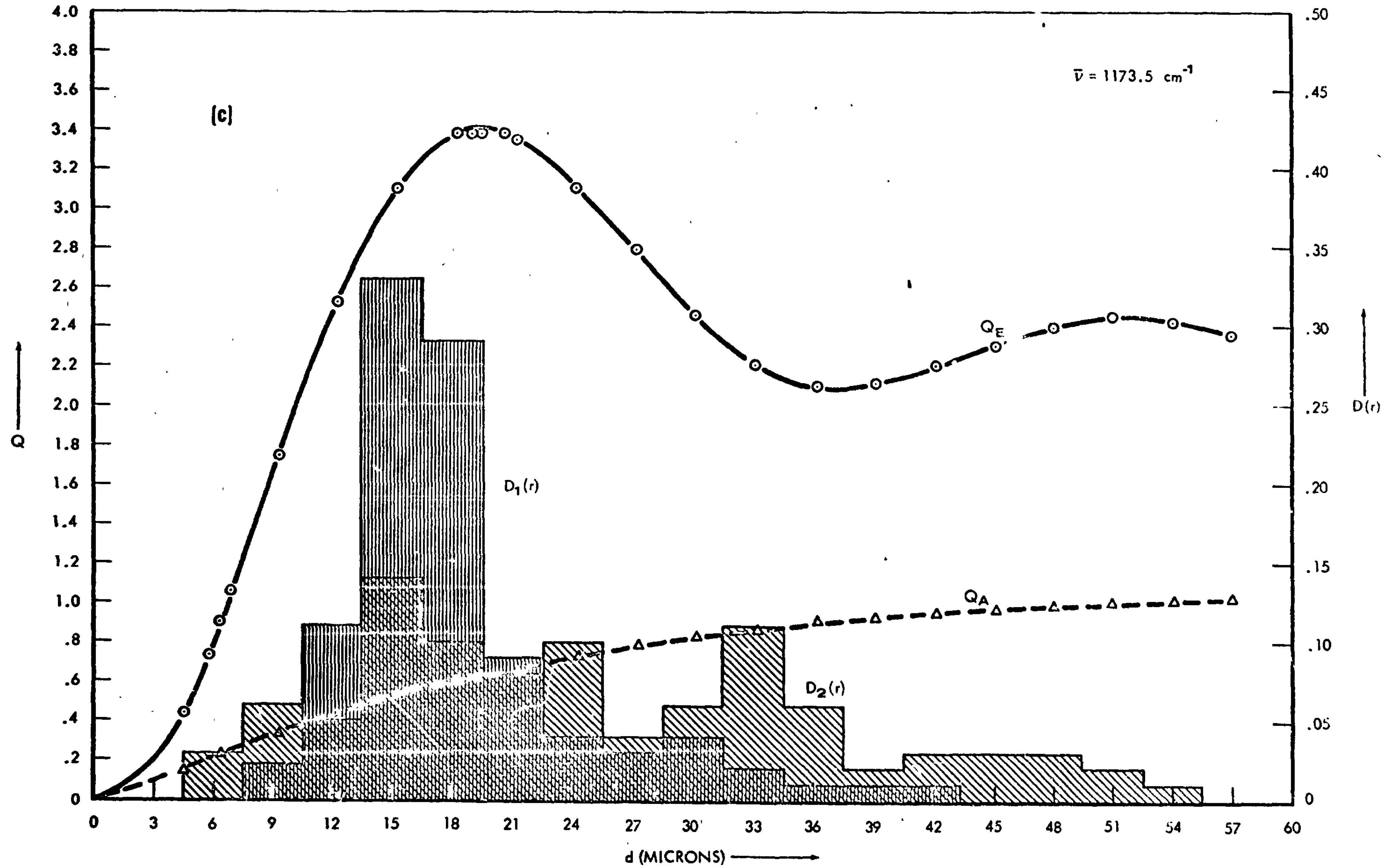

(c)
$\bar{\nu}$ = 1173.5 cm^{-1}
Q
D(r)
Q_E
Q_A
$D_1(r)$
$D_2(r)$
d (MICRONS)
4.0
3.8
3.6
3.4
3.2
3.0
2.8
2.6
2.4
2.2
2.0
1.8
1.6
1.4
1.2
1.0
.8
.6
.4
.2
0
.50
.45
.40
.35
.30
.25
.20
.15
.10
.05
0
3
6
9
12
15
18
21
24
27
30
33
36
39
42
45
48
51
54
57
60

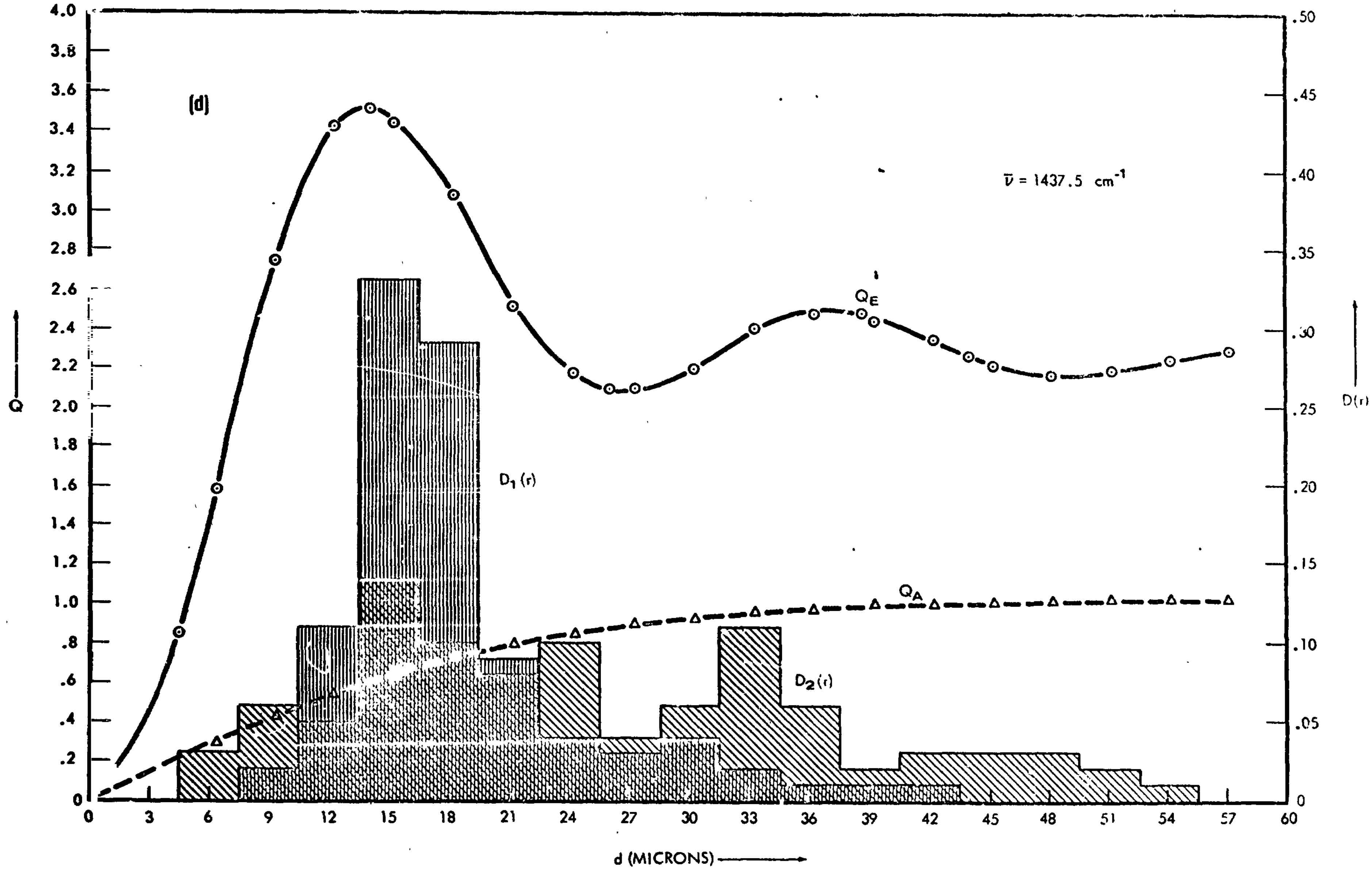
(d)
$\bar{\nu}$ = 1437.5 cm^{-1}
Q_E
Q_A
$D_1(r)$
$D_2(r)$
Q
D(r)
d (MICRONS)
4.0
3.8
3.6
3.4
3.2
3.0
2.8
2.6
2.4
2.2
2.0
1.8
1.6
1.4
1.2
1.0
.8
.6
.4
.2
0
.50
.45
.40
.35
.30
.25
.20
.15
.10
.05
0
3
6
9
12
15
18
21
24
27
30
33
36
39
42
45
48
51
54
57
60

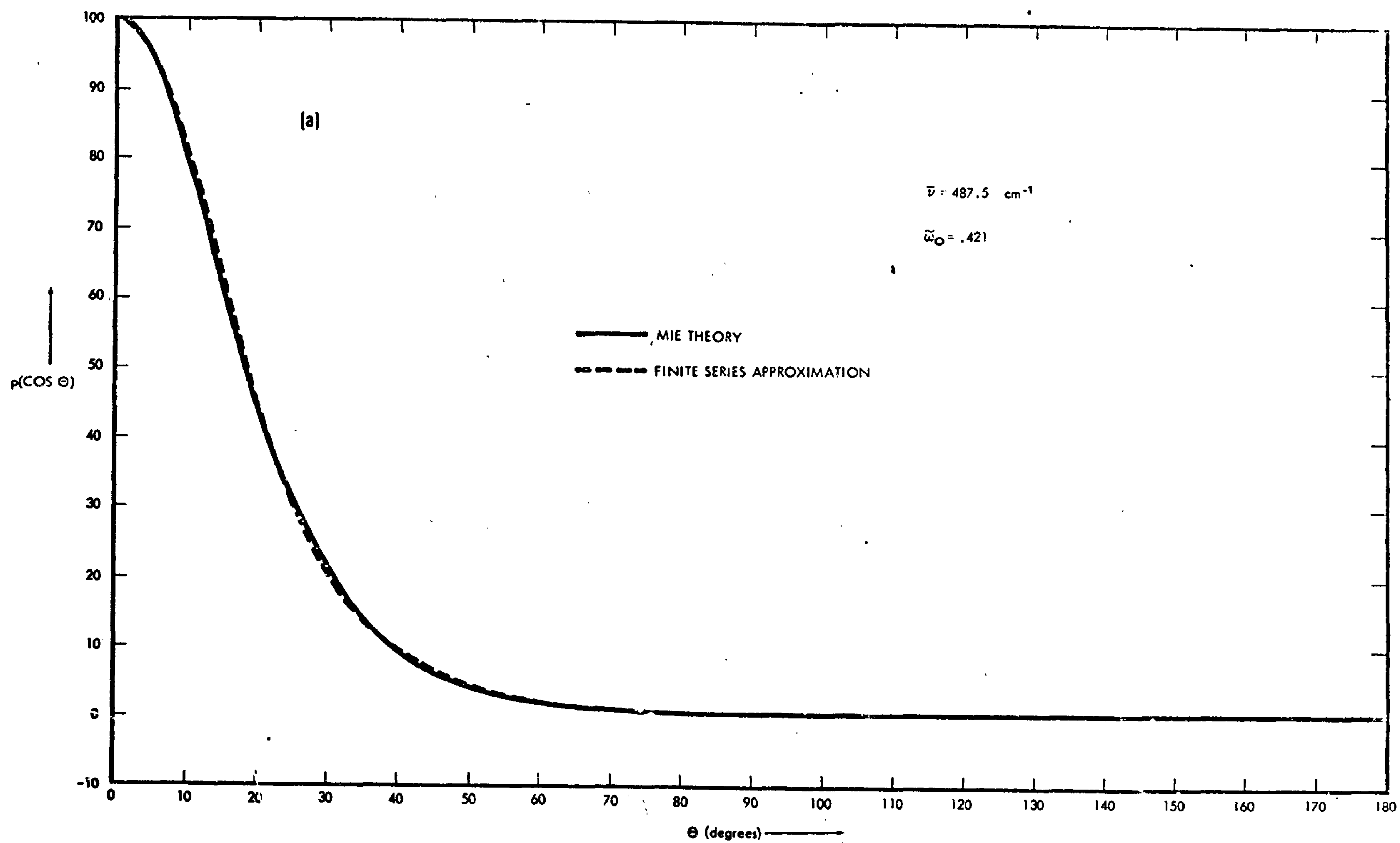
(a)
$\bar{\nu}$ = 487.5 cm^{-1}
$\tilde{\omega}_0$ = .421
MIE THEORY
FINITE SERIES APPROXIMATION
p(COS Θ)
Θ (degrees)
100
90
80
70
60
50
40
30
20
10
0
-10
0
10
20
30
40
50
60
70
80
90
100
110
120
130
140
150
160
170
180

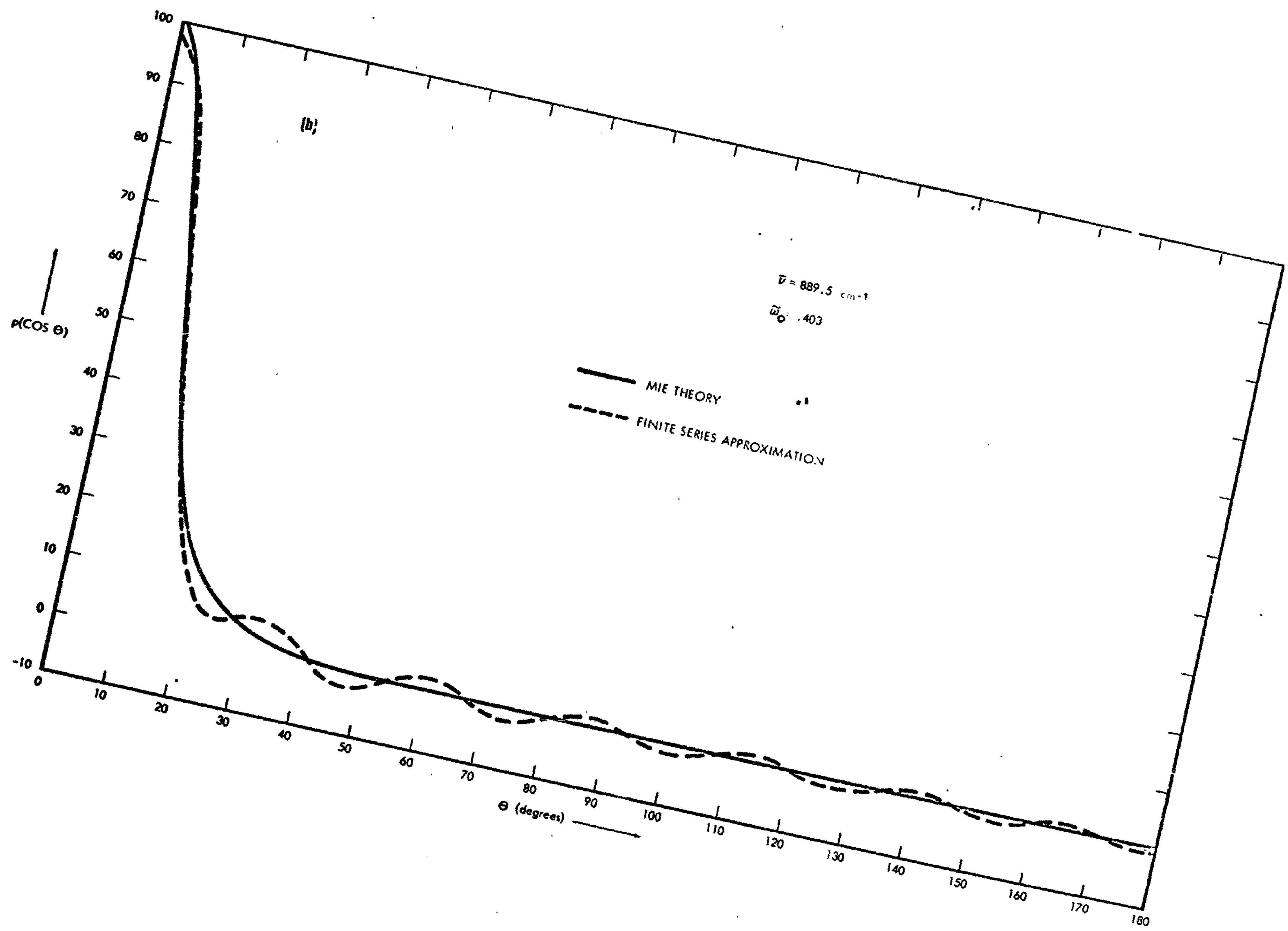

(b)
$\bar{\nu}$ = 889.5 cm-1
$\tilde{\omega}_0$: .403
MIE THEORY
FINITE SERIES APPROXIMATION
P(COS Θ)
Θ (degrees)

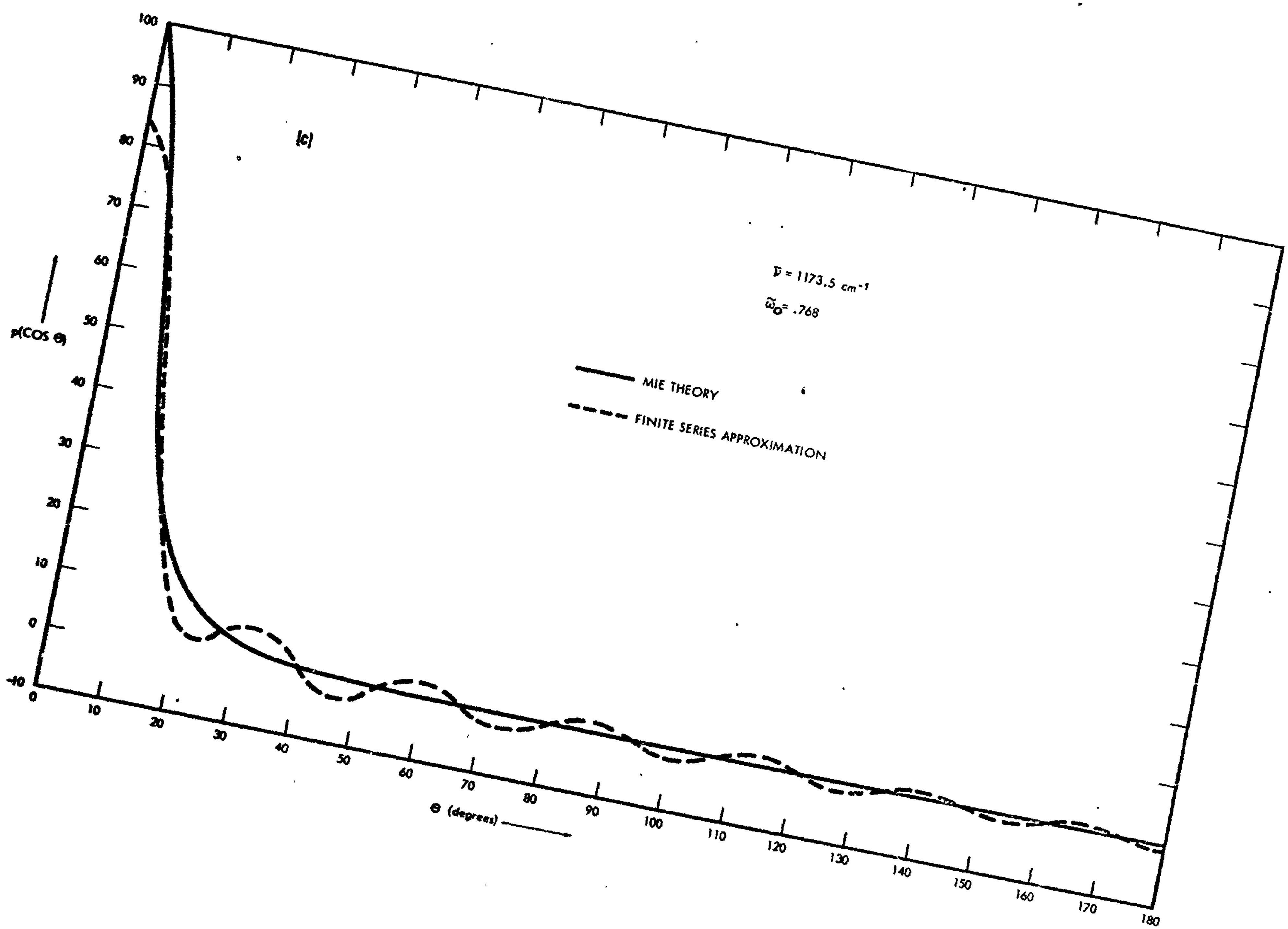
(c)
$\bar{\nu}$ = 1173.5 cm⁻¹
$\tilde{\omega}_0$ = .768
MIE THEORY
FINITE SERIES APPROXIMATION
p(COS Θ)
Θ (degrees)
100
90
80
70
60
50
40
30
20
10
0
-10
0
10
20
30
40
50
60
70
80
90
100
110
120
130
140
150
160
170
180

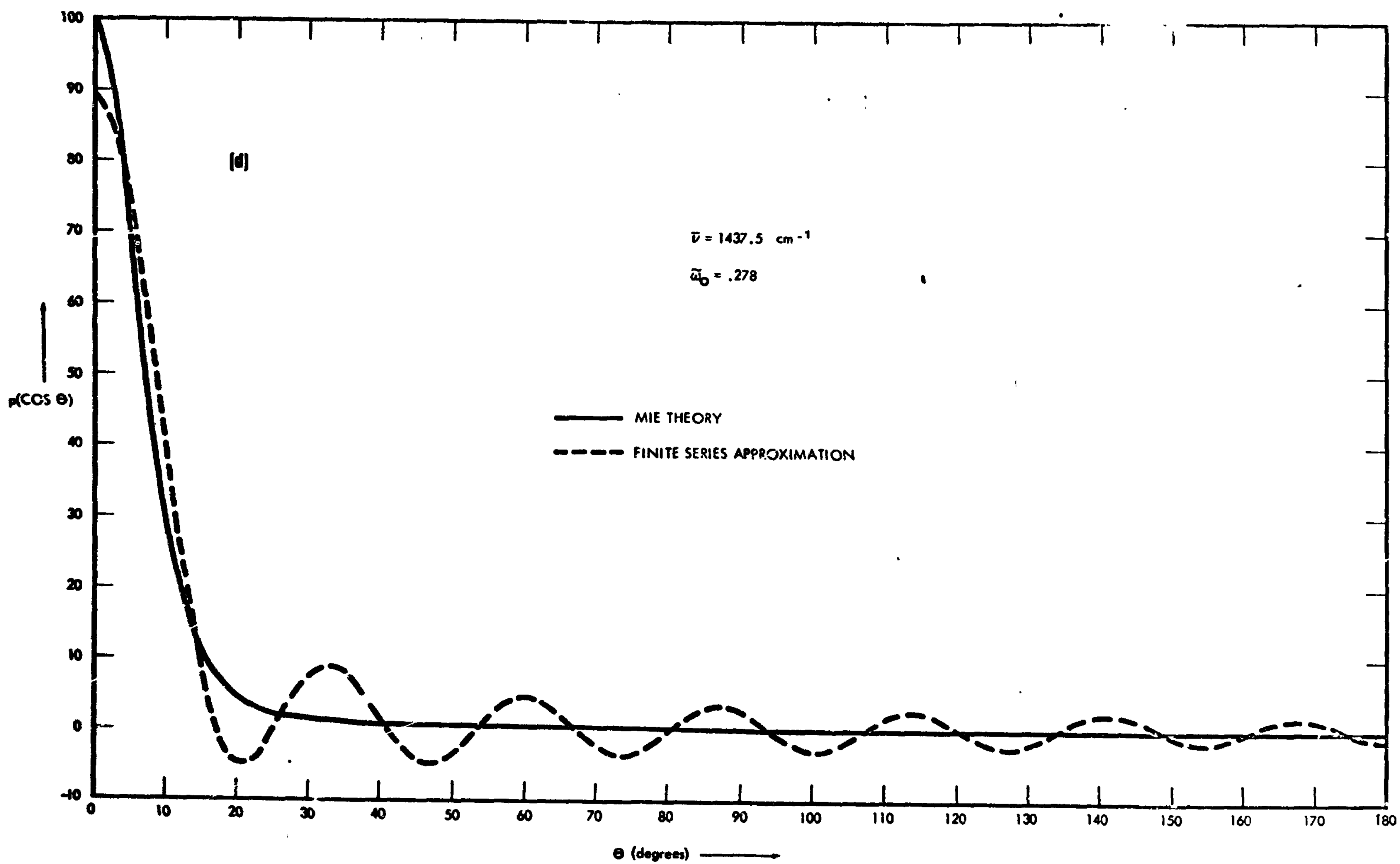

(d)
$\bar{\nu}$ = 1437.5 cm^{-1}
$\tilde{\omega}_0$ = .278
MIE THEORY
FINITE SERIES APPROXIMATION
p(COS Θ)
Θ (degrees)
100
90
80
70
60
50
40
30
20
10
0
-10
0
10
20
30
40
50
60
70
80
90
100
110
120
130
140
150
160
170
180

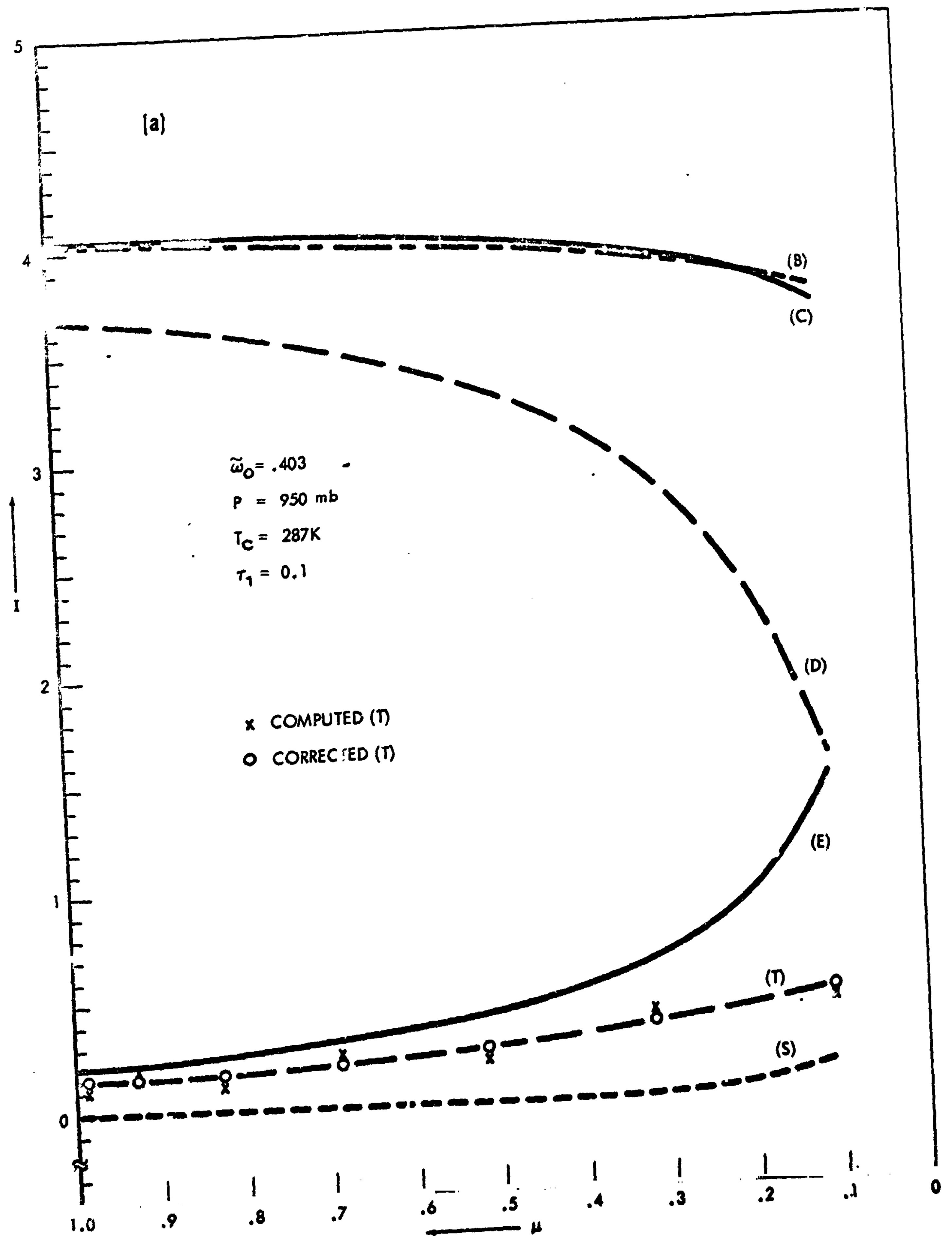

5
[a]
4
(B)
(C)
3
$\tilde{\omega}_0$ = .403
P = 950 mb
T_C = 287K
τ_1 = 0.1
I
2
(D)
x COMPUTED (T)
O CORREC:ED (T)
(E)
1
(T)
(S)
0
1.0
.9
.8
.7
.6
.5
.4
.3
.2
.1
0
μ

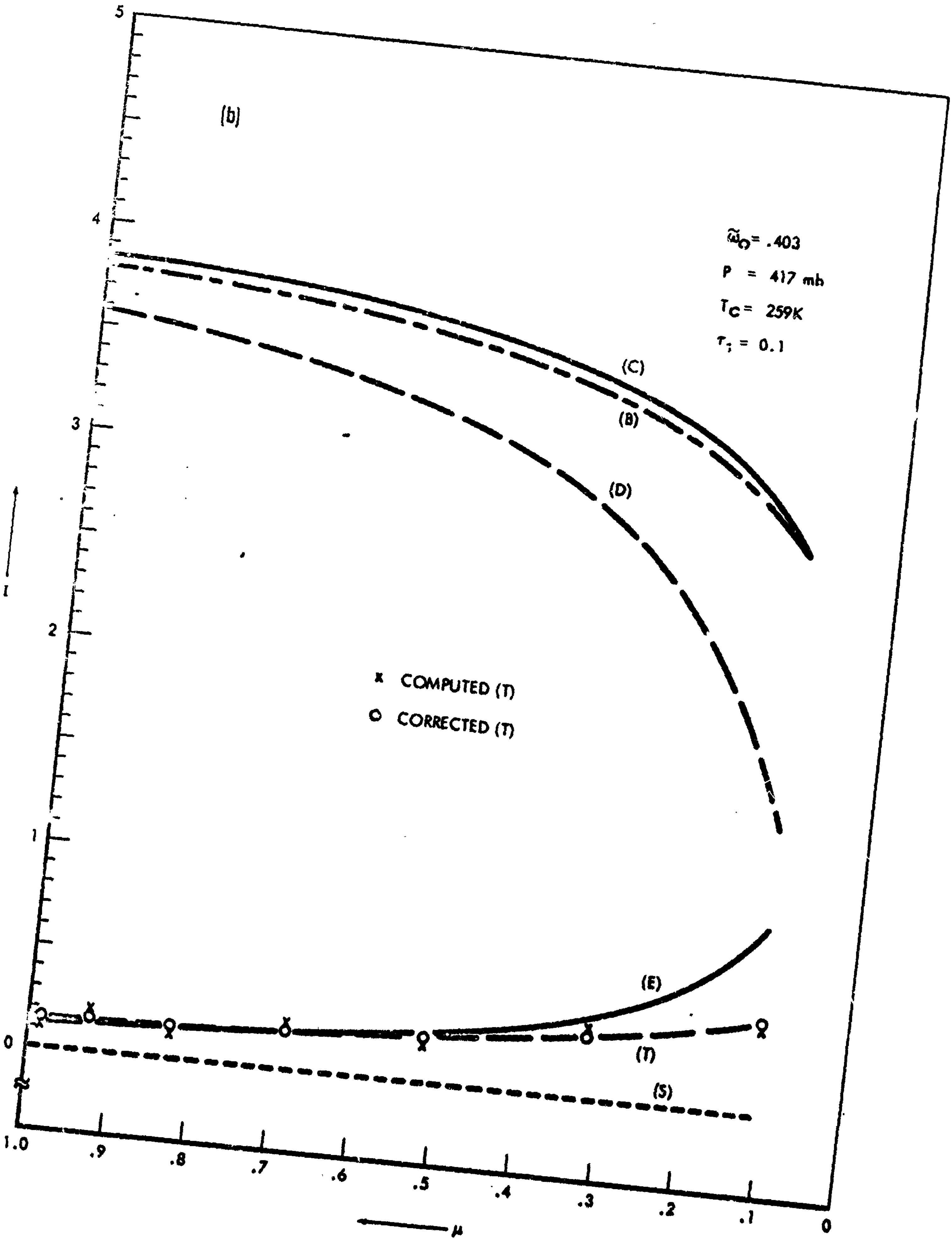

(b)
$\tilde{\omega}_o$ = .403
P = 417 mb
T_c = 259K
τ_1 = 0.1
(C)
(B)
(D)
(E)
(T)
(S)
x COMPUTED (T)
o CORRECTED (T)
I
μ
5
4
3
2
1
0
1.0
.9
.8
.7
.6
.5
.4
.3
.2
.1
0

Fig.

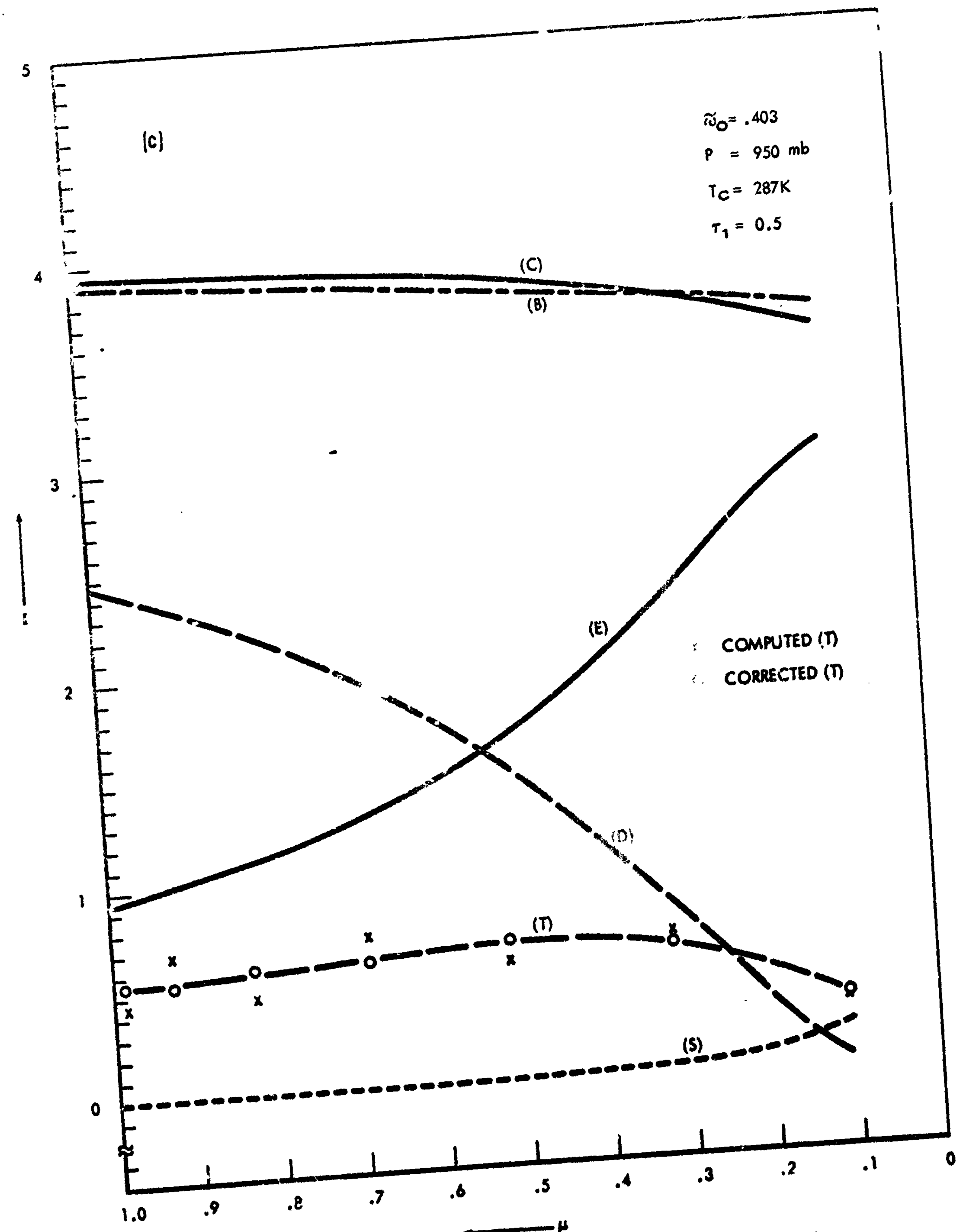
(c)
$\tilde{\omega}_0$ = .403
P = 950 mb
T_C = 287K
τ_1 = 0.5
(C)
(B)
(E)
(D)
(T)
(S)
COMPUTED (T)
CORRECTED (T)
μ

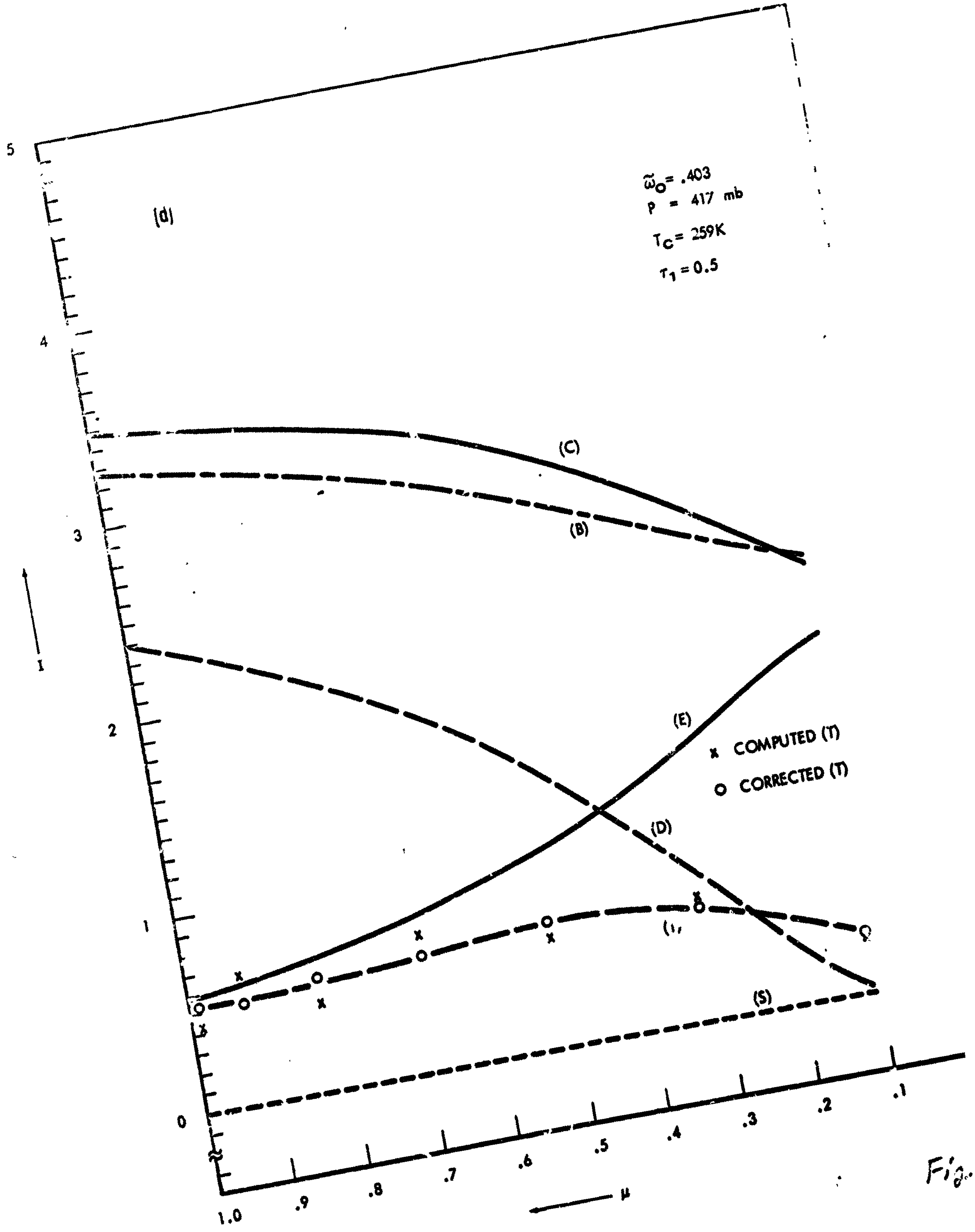

(d)
$\tilde{\omega}_0 = .403$
P = 417 mb
$T_C = 259K$
$\tau_1 = 0.5$
(C)
(B)
(E)
(D)
(S)
x COMPUTED (T)
o CORRECTED (T)
I
μ
5
4
3
2
1
0
1.0
.9
.8
.7
.6
.5
.4
.3
.2
.1

Fig.

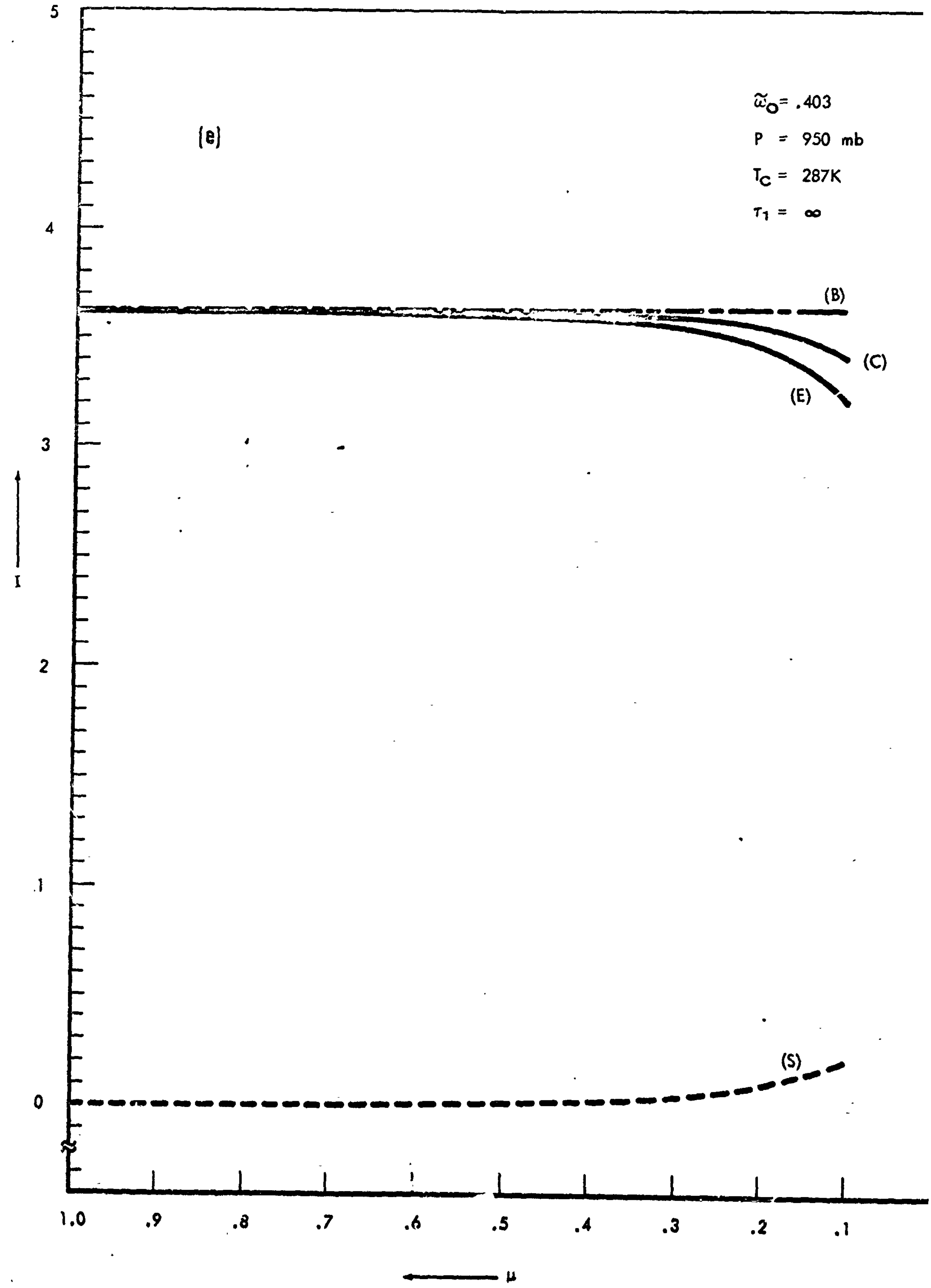

5
4
3
2
1
0
I
(e)
$\tilde{\omega}_0 = .403$
P = 950 mb
T_C = 287K
$\tau_1 = \infty$
(B)
(C)
(E)
(S)
1.0
.9
.8
.7
.6
.5
.4
.3
.2
.1
μ

F.

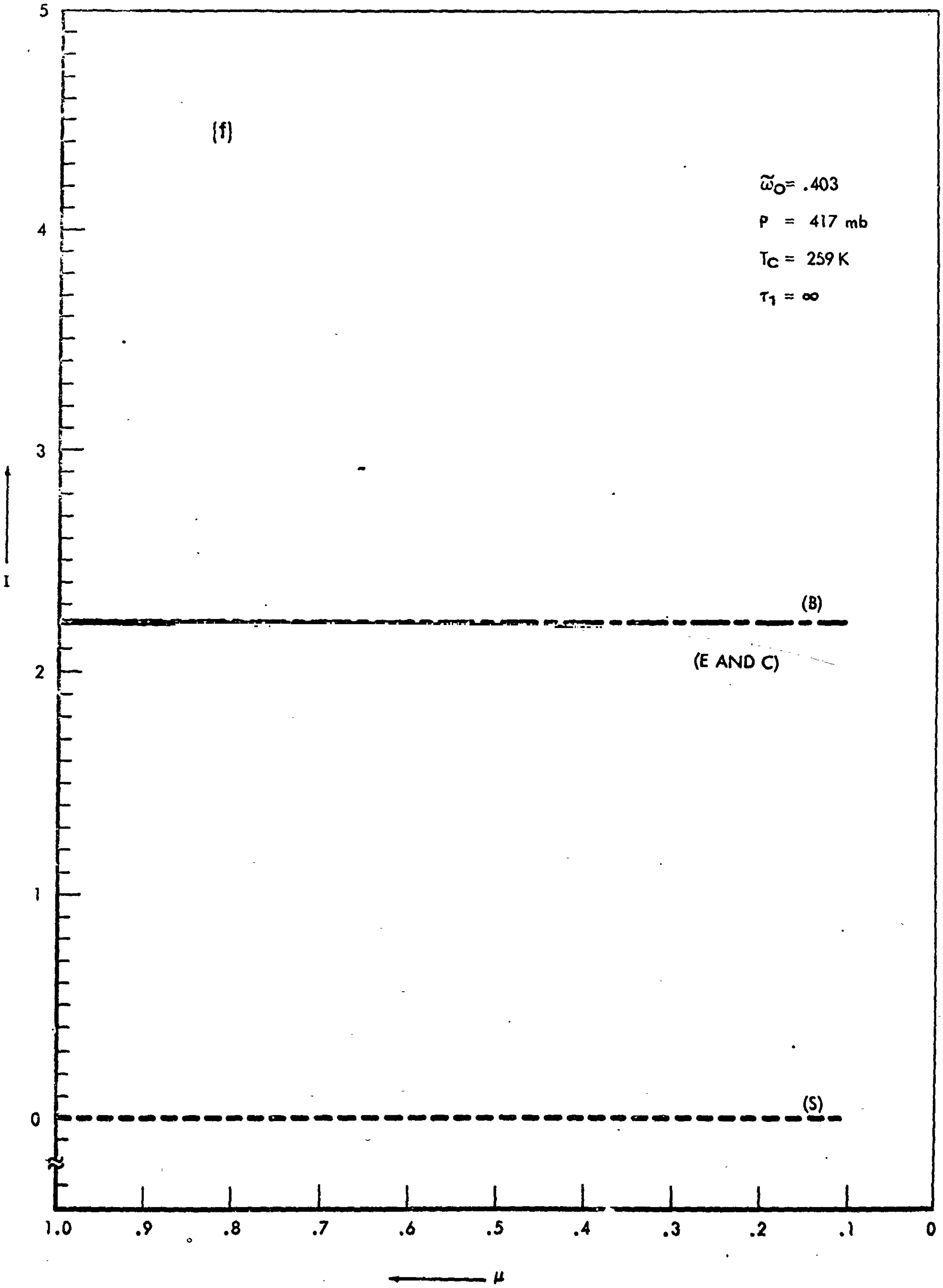
(f)
$\tilde{\omega}_O$ = .403
P = 417 mb
T_C = 259 K
τ_1 = ∞
(B)
(E AND C)
(S)
I
5
4
3
2
1
0
1.0
.9
.8
.7
.6
.5
.4
.3
.2
.1
0
μ

Fig. 4

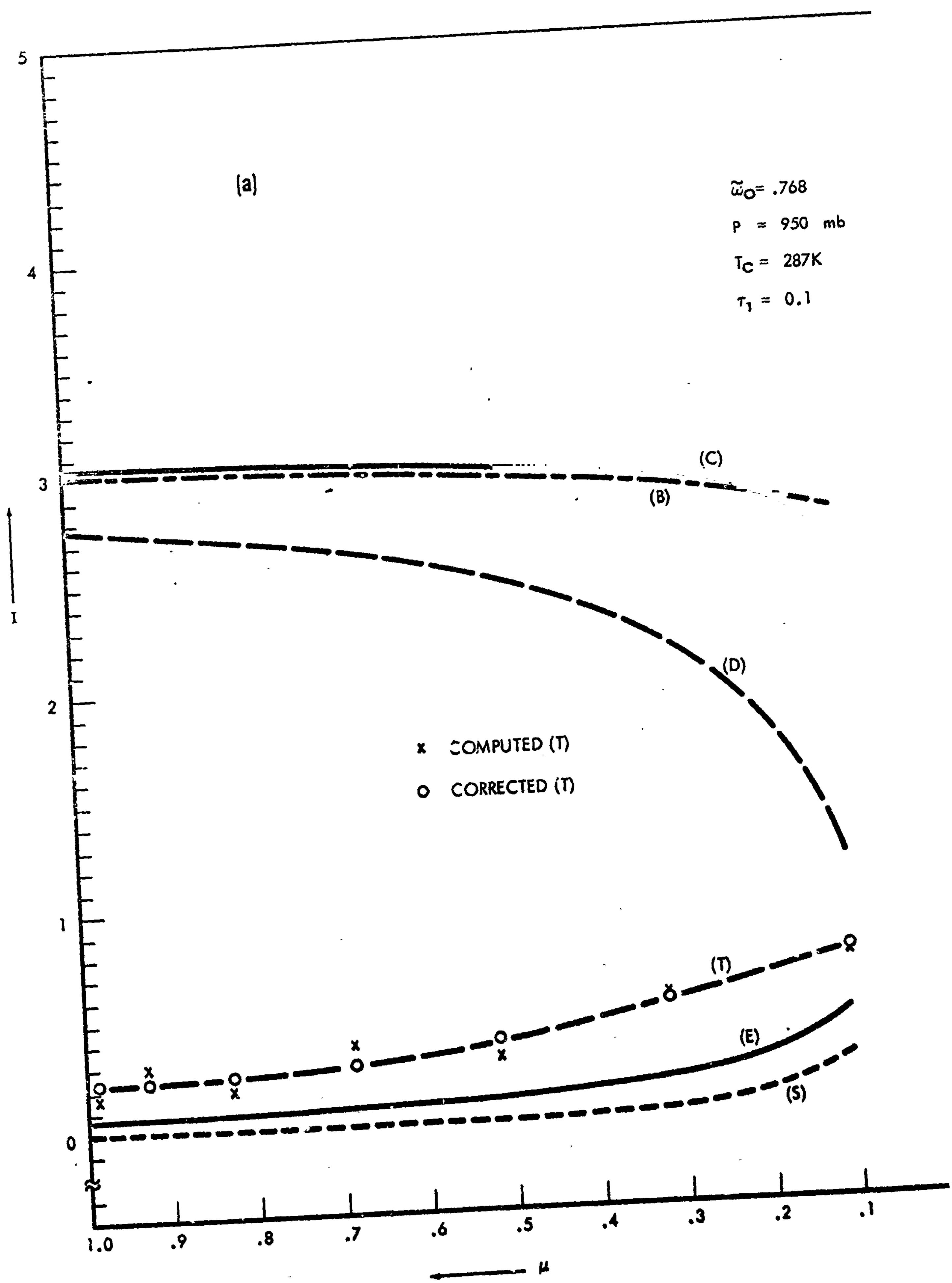

(a)
$\tilde{\omega}_O$= .768
p = 950 mb
T_C = 287K
τ_1 = 0.1
(C)
(B)
(D)
x COMPUTED (T)
o CORRECTED (T)
(T)
(E)
(S)
I
μ
5
4
3
2
1
0
1.0
.9
.8
.7
.6
.5
.4
.3
.2
.1

Fig

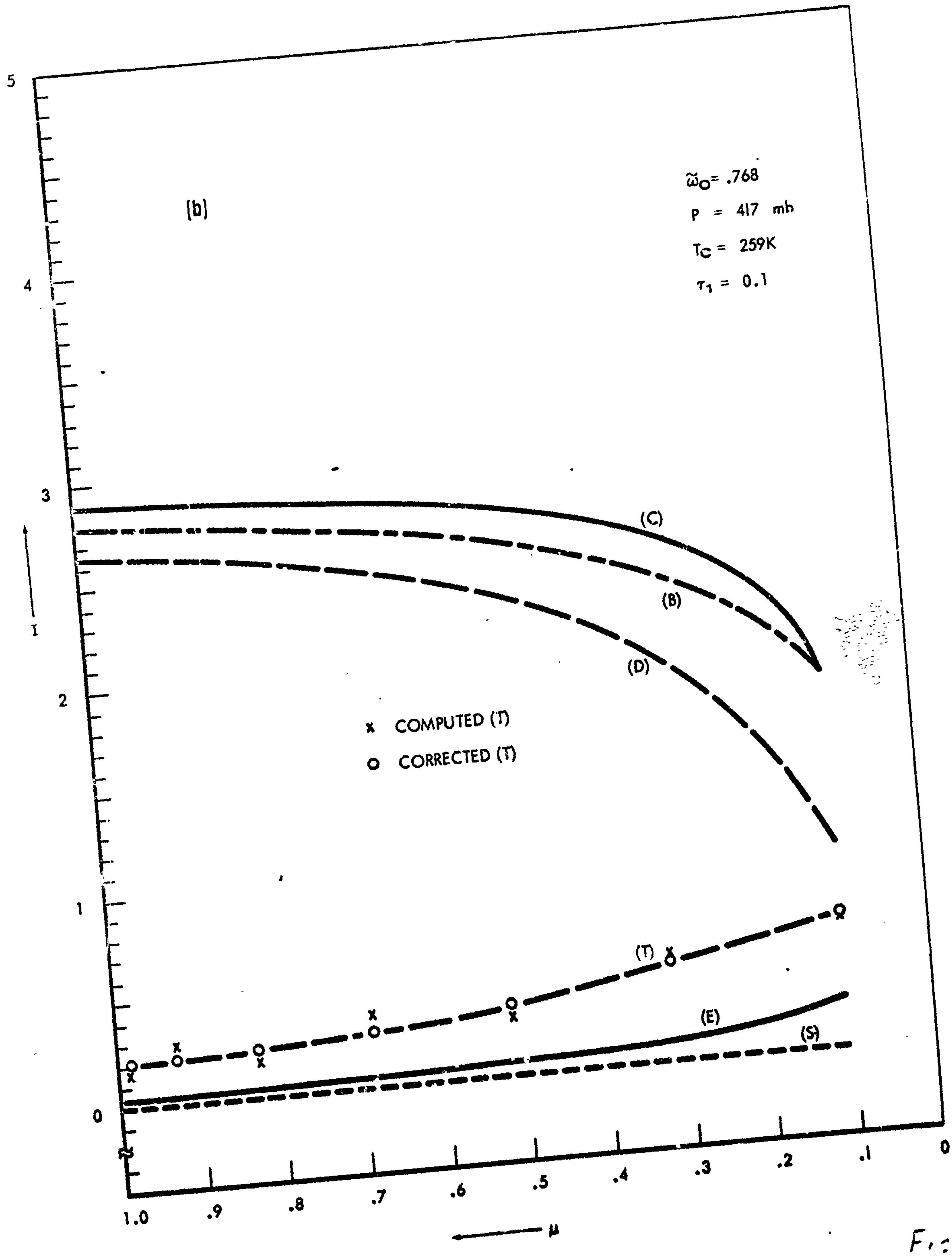
(b)
$\tilde{\omega}_O$ = .768
p = 417 mb
T_C = 259K
τ_1 = 0.1
5
4
3
2
1
0
I
(C)
(B)
(D)
x COMPUTED (T)
o CORRECTED (T)
(T)
(E)
(S)
1.0
.9
.8
.7
.6
.5
.4
.3
.2
.1
0
μ

Fig 5

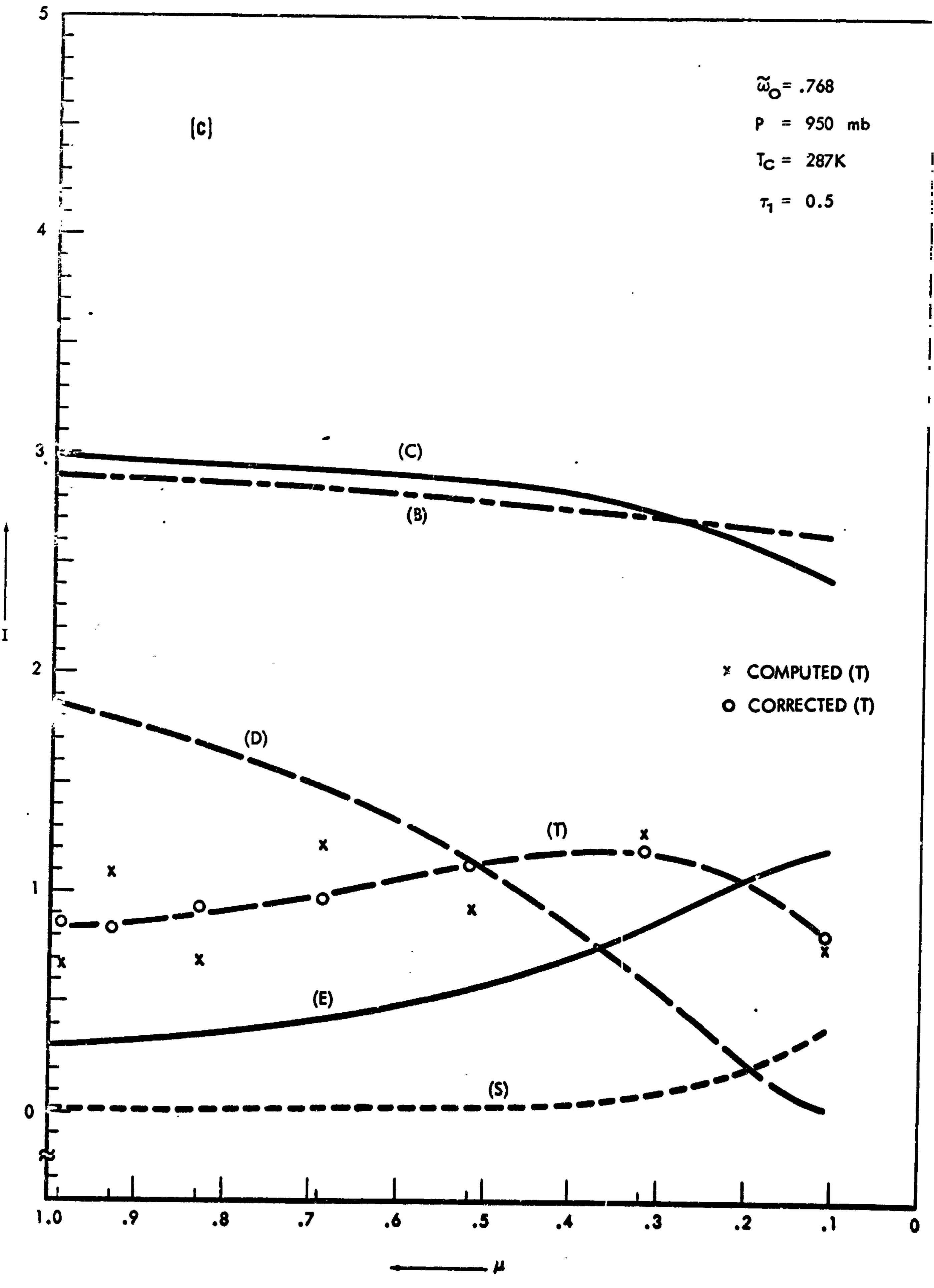

(c)
$\tilde{\omega}_O$ = .768
P = 950 mb
T_C = 287K
τ_1 = 0.5
(C)
(B)
(D)
(T)
(E)
(S)
x COMPUTED (T)
O CORRECTED (T)
I
μ
5
4
3
2
1
0
1.0
.9
.8
.7
.6
.5
.4
.3
.2
.1
0

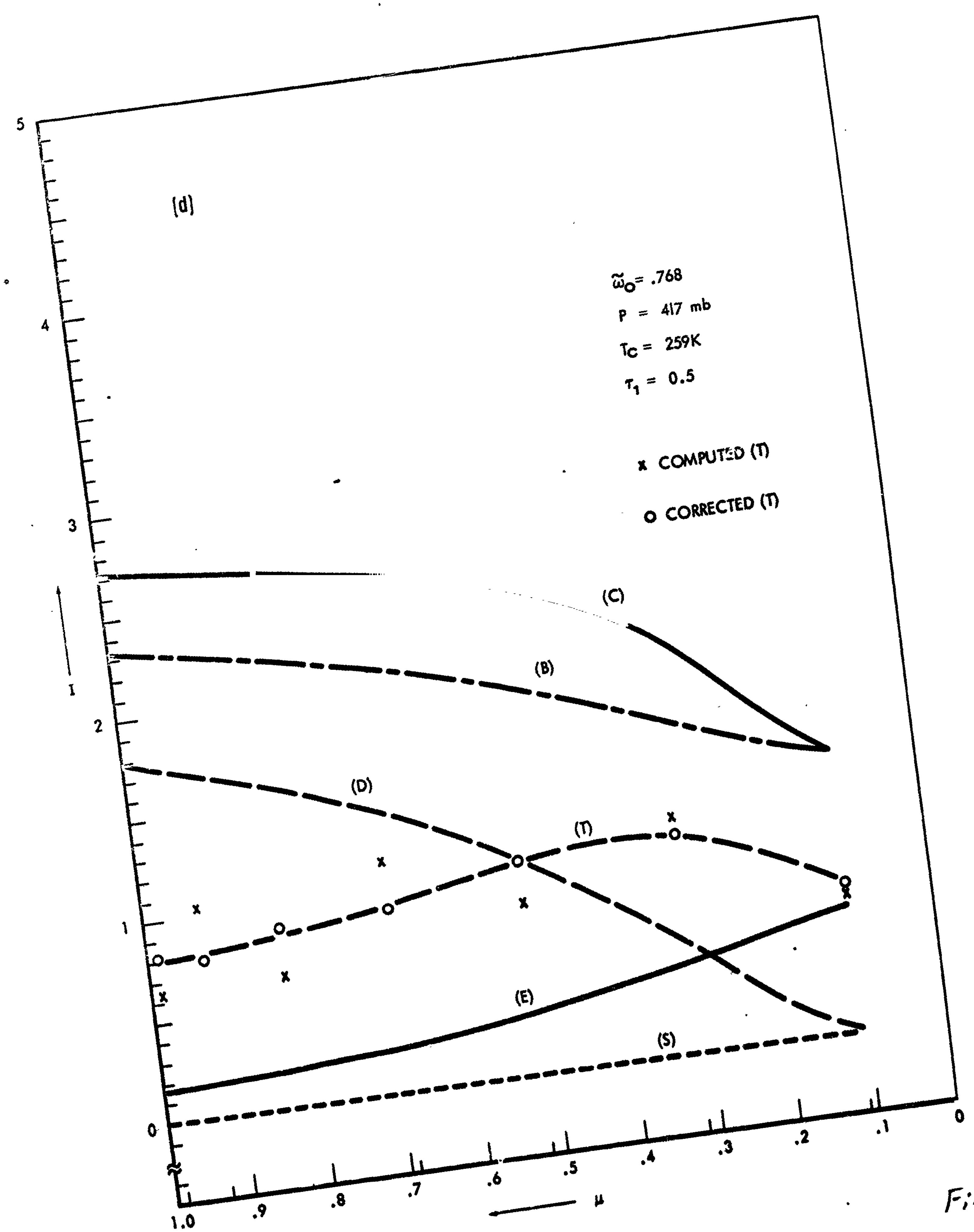

[d]
$\tilde{\omega}_0$ = .768
P = 417 mb
T_C = 259K
τ_1 = 0.5
x COMPUTED (T)
o CORRECTED (T)
(C)
(B)
(D)
(T)
(E)
(S)
I
μ
5
4
3
2
1
0
1.0
.9
.8
.7
.6
.5
.4
.3
.2
.1
0

Fig C

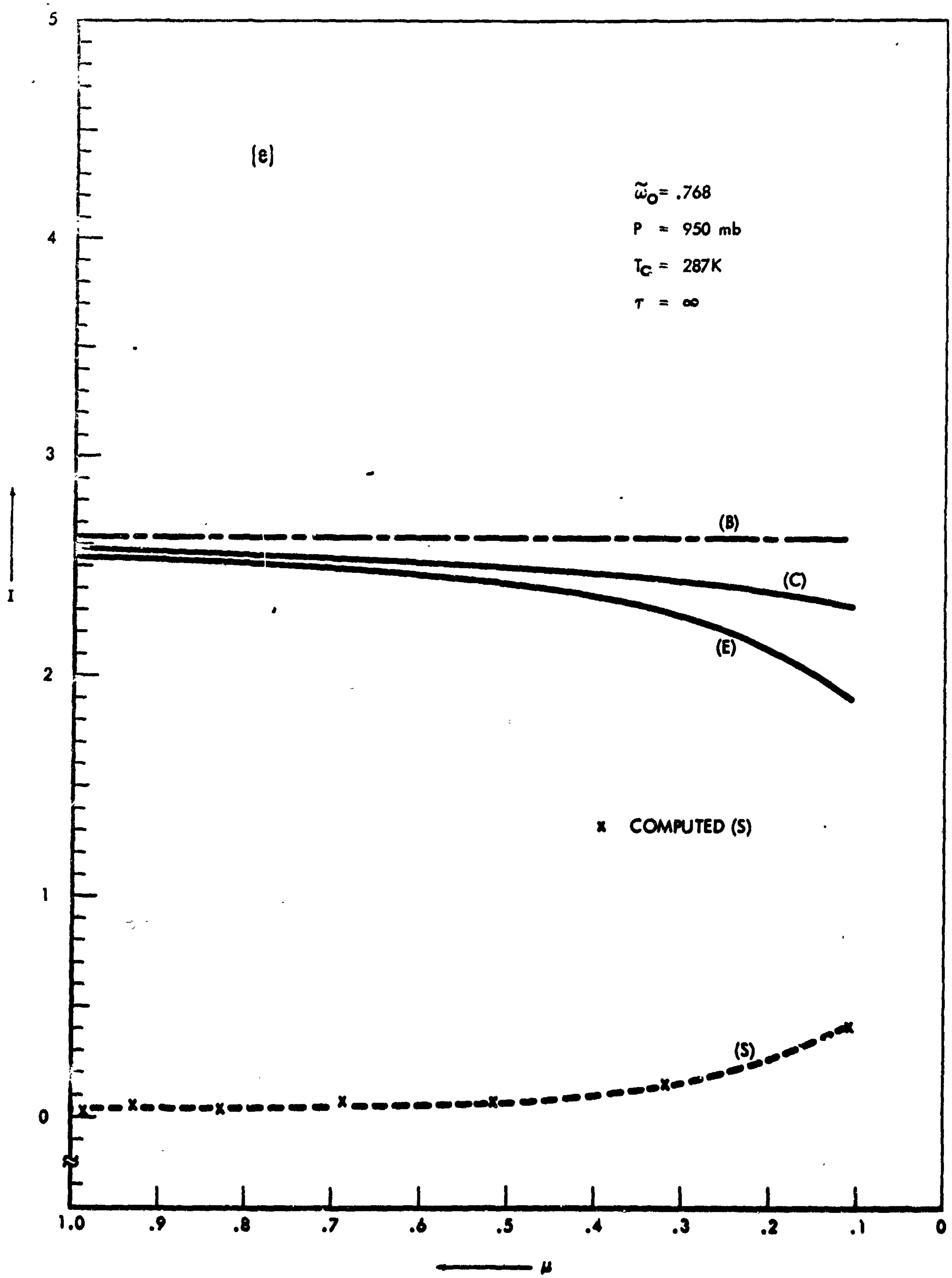

(e)
$\tilde{\omega}_0$ = .768
P = 950 mb
T_C = 287K
τ = ∞
(B)
(C)
(E)
x COMPUTED (S)
(S)
I
5
4
3
2
1
0
1.0
.9
.8
.7
.6
.5
.4
.3
.2
.1
0
μ

E.

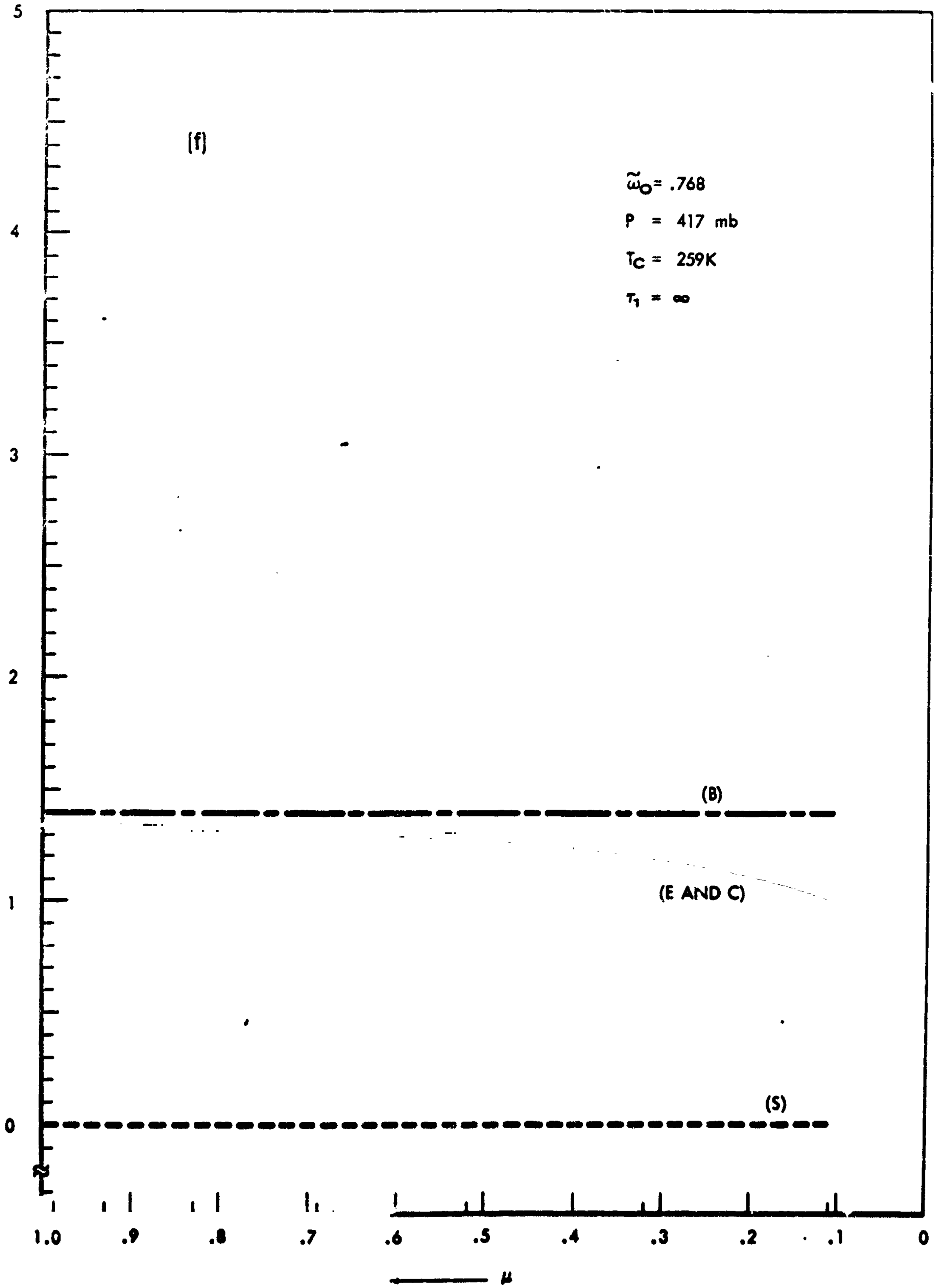

5
4
3
2
1
0
(f)
$\tilde{\omega}_0$ = .768
P = 417 mb
T_C = 259K
τ_1 = ∞
(B)
(E AND C)
(S)
1.0
.9
.8
.7
.6
.5
.4
.3
.2
.1
0
μ

Fig. 5

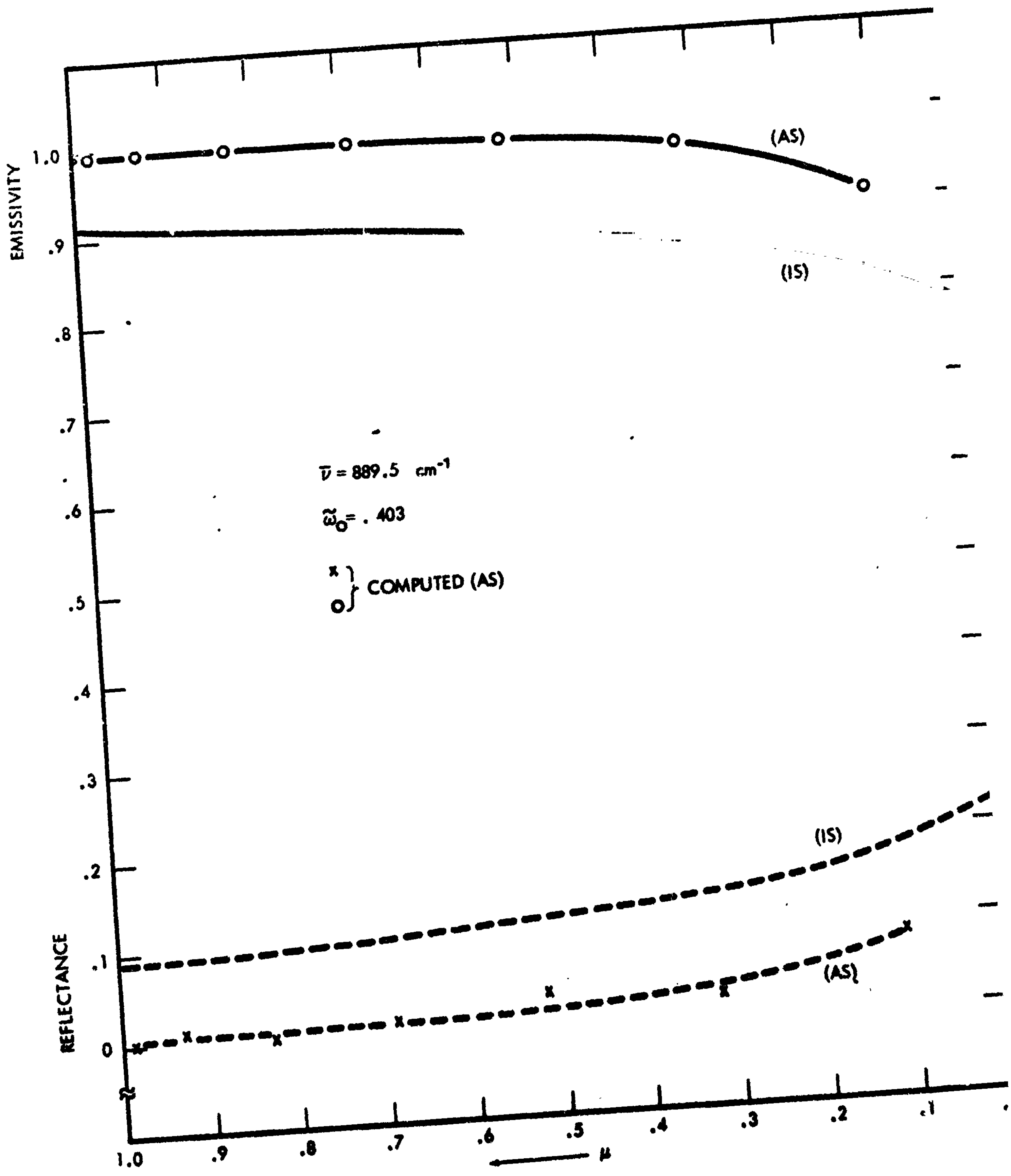

EMISSIVITY
REFLECTANCE
1.0
.9
.8
.7
.6
.5
.4
.3
.2
.1
0
(AS)
(IS)
(IS)
(AS)
$\bar{\nu}$ = 889.5 cm^{-1}
$\tilde{\omega}_0$ = .403
x
o
COMPUTED (AS)
1.0
.9
.8
.7
.6
.5
.4
.3
.2
.1
μ

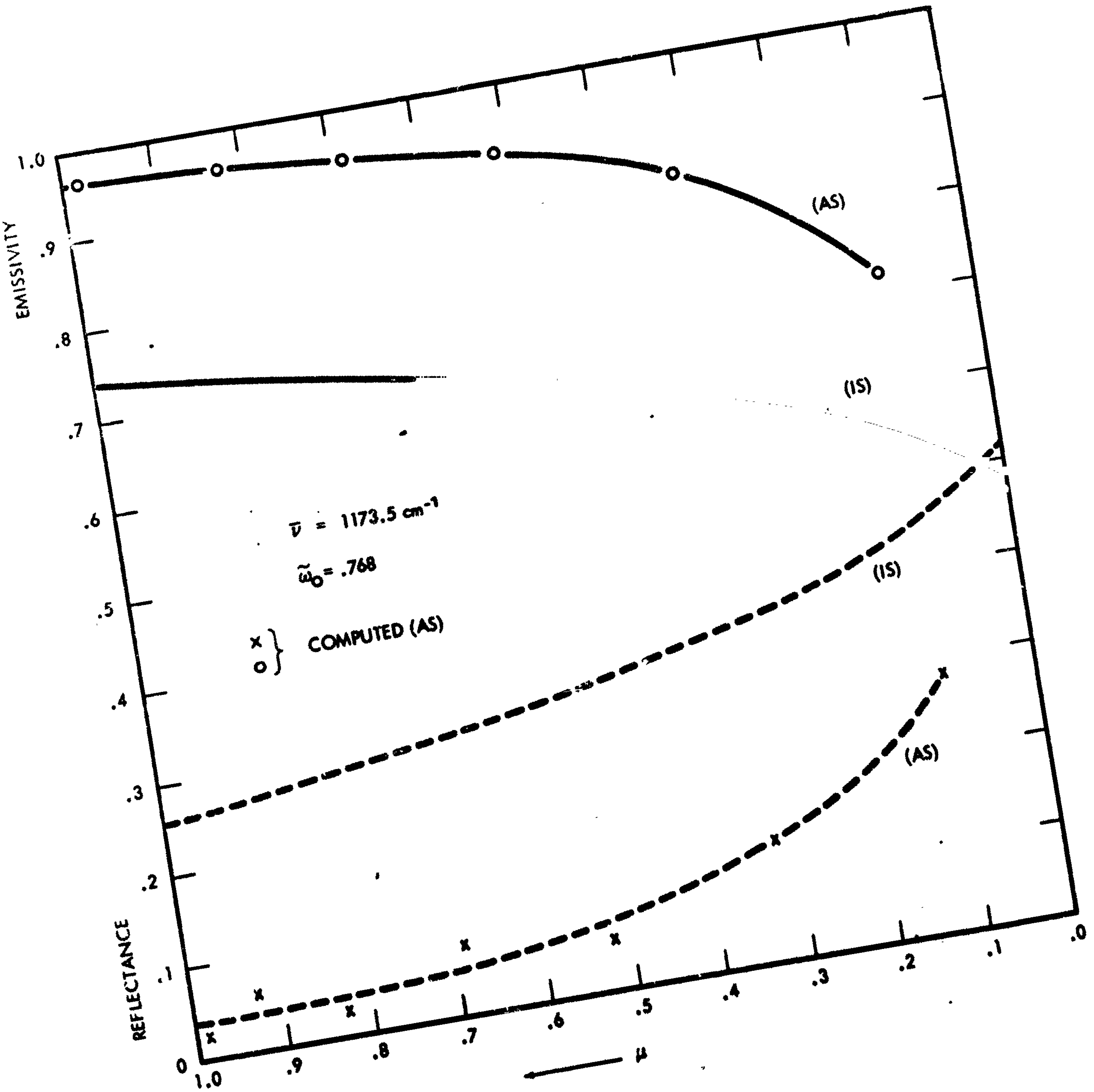

EMISSIVITY
REFLECTANCE
1.0
.9
.8
.7
.6
.5
.4
.3
.2
.1
0
1.0
.9
.8
.7
.6
.5
.4
.3
.2
.1
.0
μ
(AS)
(IS)
(IS)
(AS)
$\bar{\nu}$ = 1173.5 cm-1
$\tilde{\omega}_o$ = .768
x
o
COMPUTED (AS)

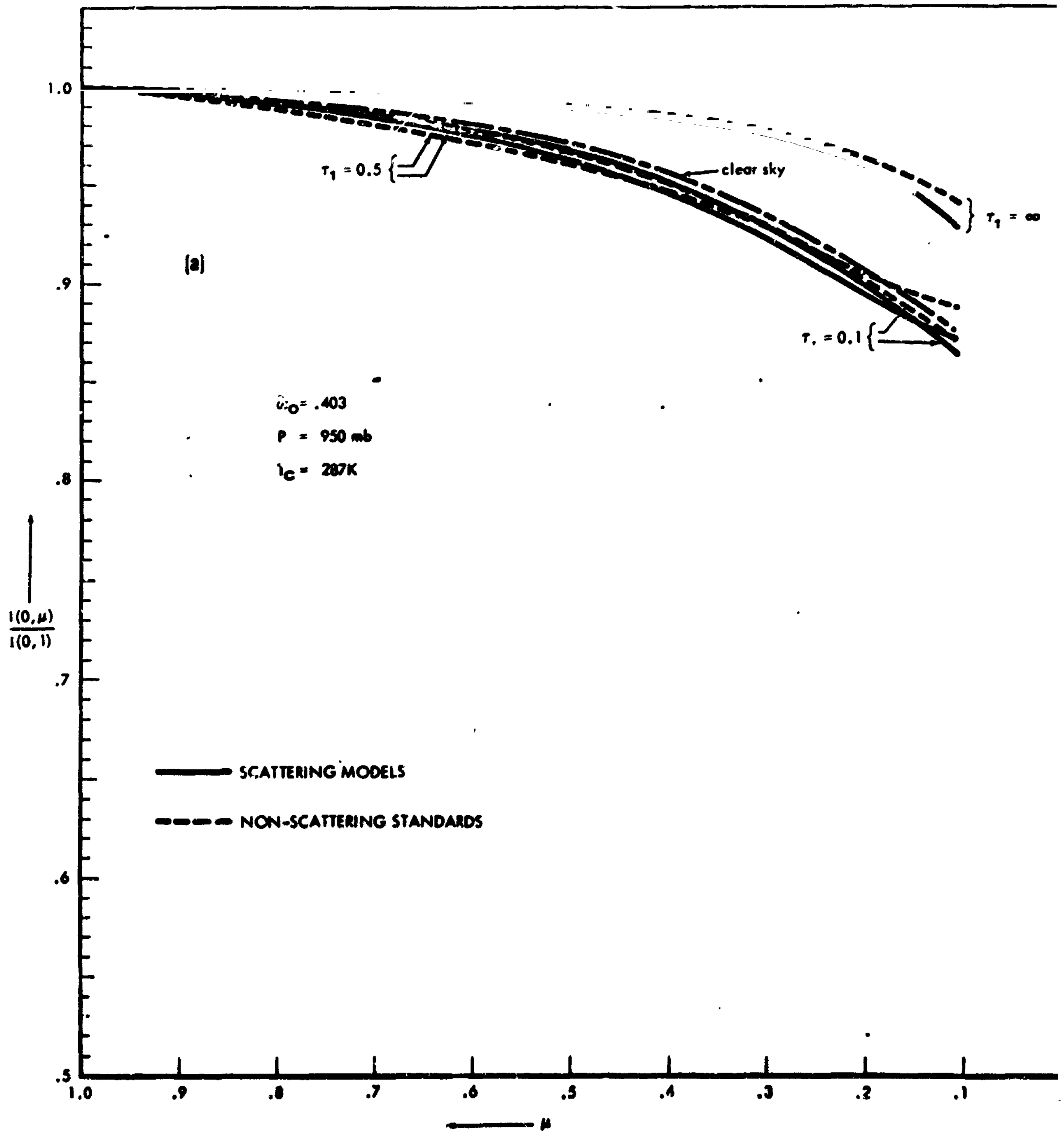

1.0
.9
.8
.7
.6
.5
$\frac{I(0,\mu)}{I(0,1)}$
$\tau_1 = 0.5$
clear sky
$\tau_1 = \infty$
(a)
$\tau_1 = 0.1$
ω_o = .403
P = 950 mb
T_C = 287K
SCATTERING MODELS
NON-SCATTERING STANDARDS
1.0
.9
.8
.7
.6
.5
.4
.3
.2
.1
μ

Fig.

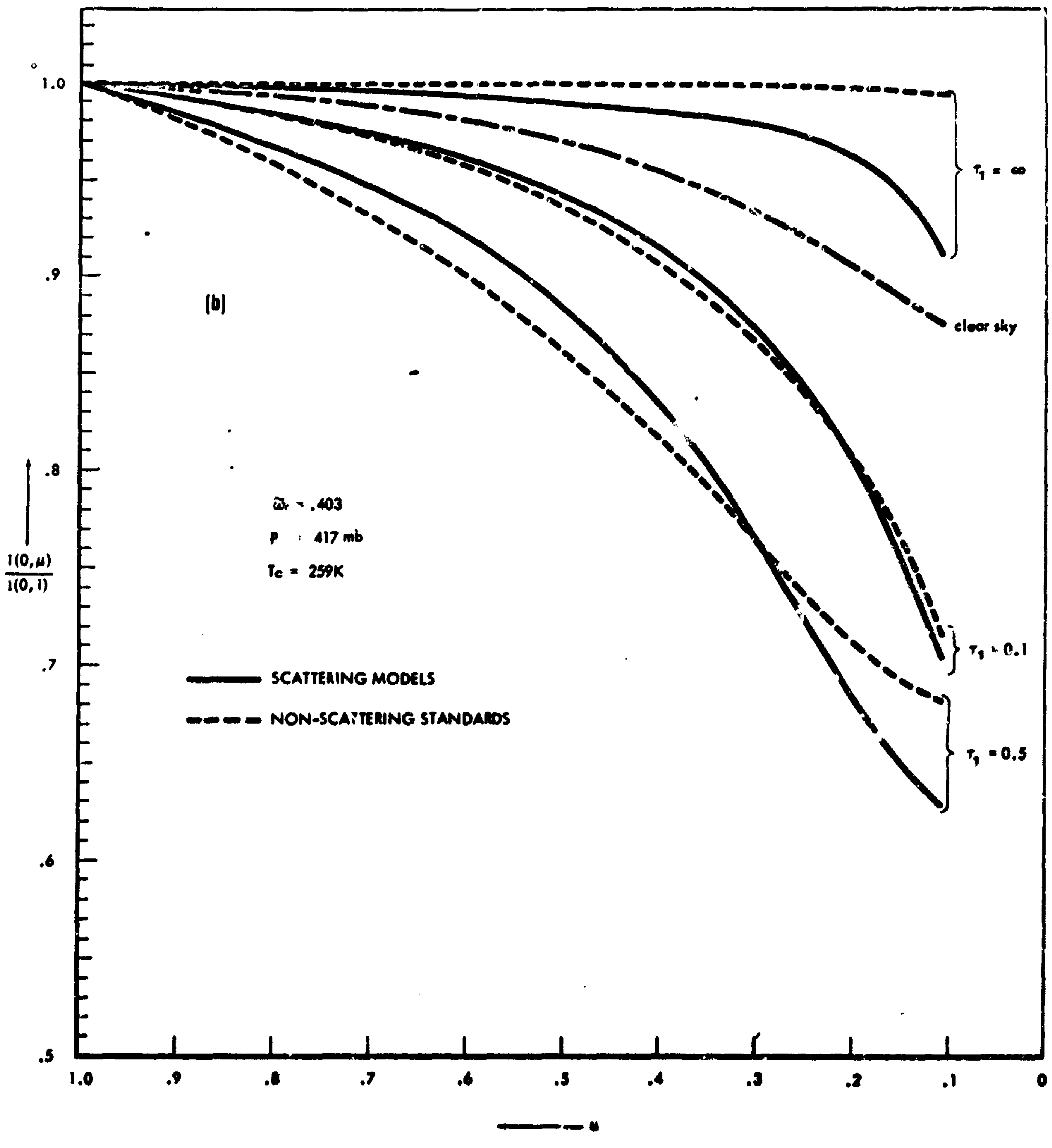
1.0
.9
.8
.7
.6
.5
$\frac{I(0,\mu)}{I(0,1)}$
(b)
$\tilde{\omega}_r$ = .403
P : 417 mb
T_c = 259K
SCATTERING MODELS
NON-SCATTERING STANDARDS
$\tau_1 = \infty$
clear sky
τ_1 = 0.1
τ_1 = 0.5
1.0
.9
.8
.7
.6
.5
.4
.3
.2
.1
0
μ

Fig.

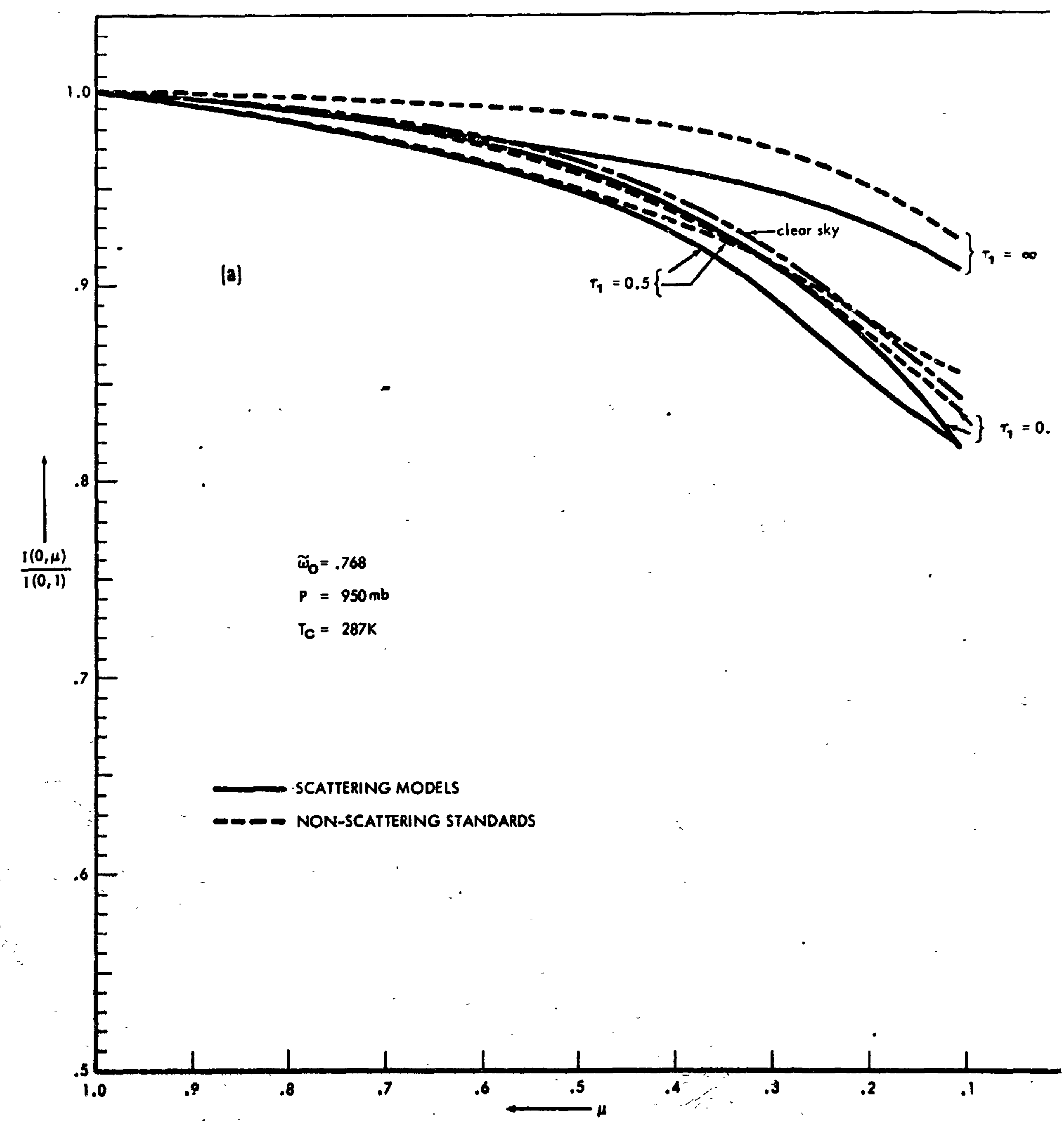
1.0
.9
.8
.7
.6
.5
(a)
clear sky
$\tau_1 = \infty$
$\tau_1 = 0.5$
$\tau_1 = 0.$
$\frac{I(0,\mu)}{I(0,1)}$
$\tilde{\omega}_0 = .768$
P = 950 mb
T_C = 287K
SCATTERING MODELS
NON-SCATTERING STANDARDS
1.0 .9 .8 .7 .6 .5 .4 .3 .2 .1
μ

Fig.

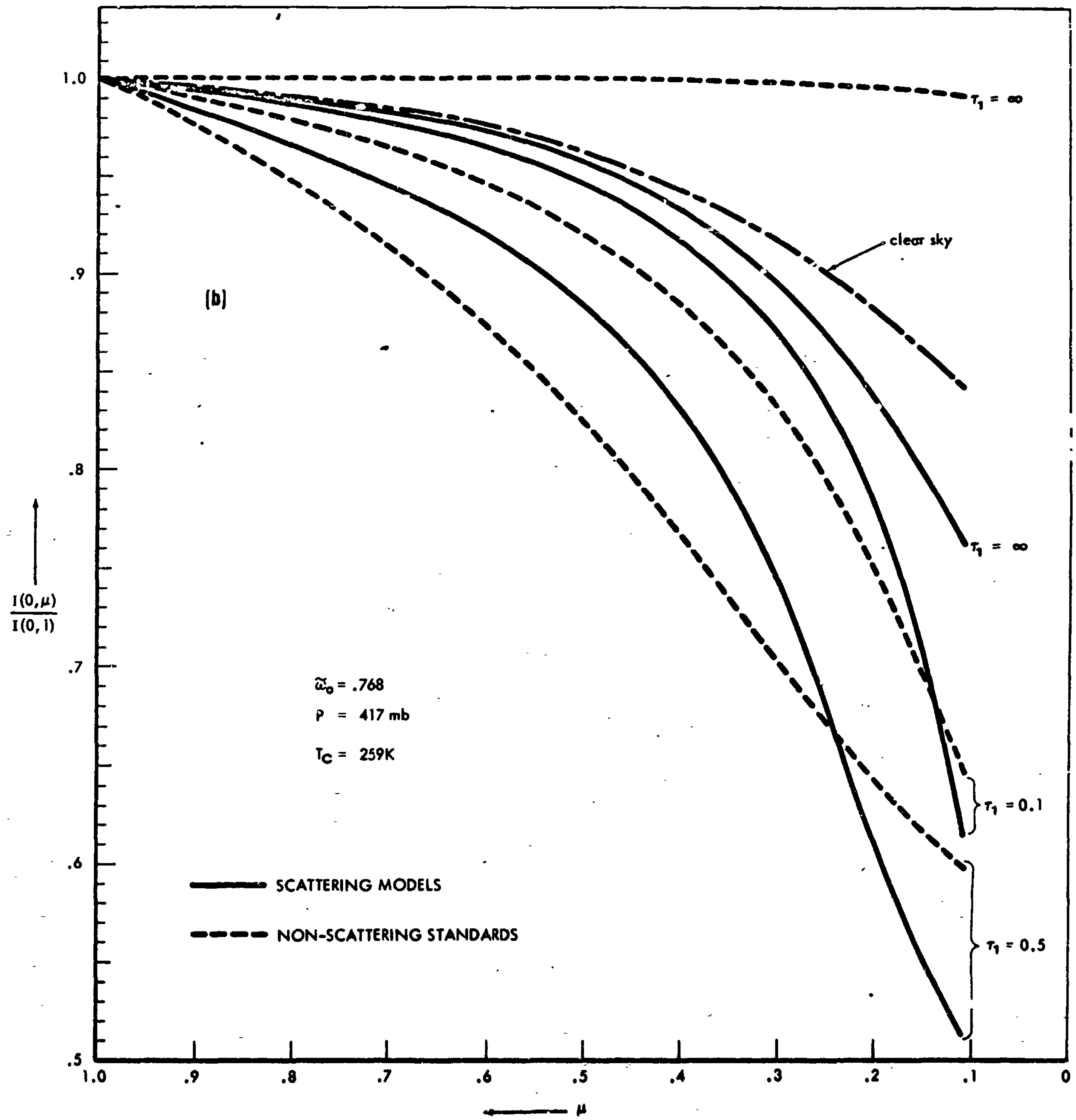
1.0
.9
.8
.7
.6
.5
I(0,μ) / I(0,1)
(b)
τ₁ = ∞
clear sky
τ₁ = ∞
τ₁ = 0.1
τ₁ = 0.5
ω̃₀ = .768
P = 417 mb
T_C = 259K
SCATTERING MODELS
NON-SCATTERING STANDARDS
1.0 .9 .8 .7 .6 .5 .4 .3 .2 .1 0
μ

Fig. 9

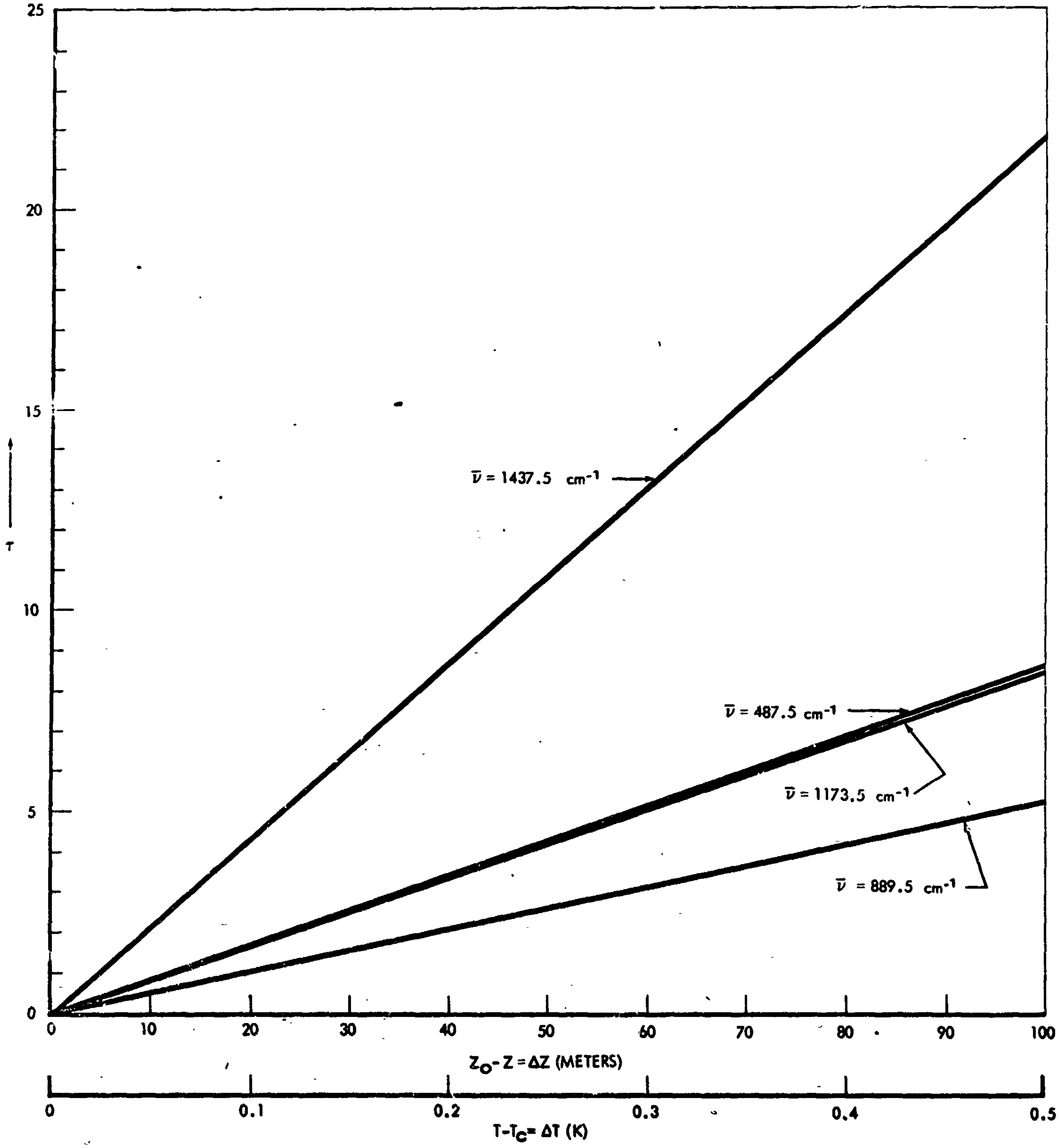

25
20
15
10
5
0
τ
$\bar{\nu}$ = 1437.5 cm^{-1}
$\bar{\nu}$ = 487.5 cm^{-1}
$\bar{\nu}$ = 1173.5 cm^{-1}
$\bar{\nu}$ = 889.5 cm^{-1}
0 10 20 30 40 50 60 70 80 90 100
$Z_O - Z = \Delta Z$ (METERS)
0 0.1 0.2 0.3 0.4 0.5
$T - T_C = \Delta T$ (K)

Fig.

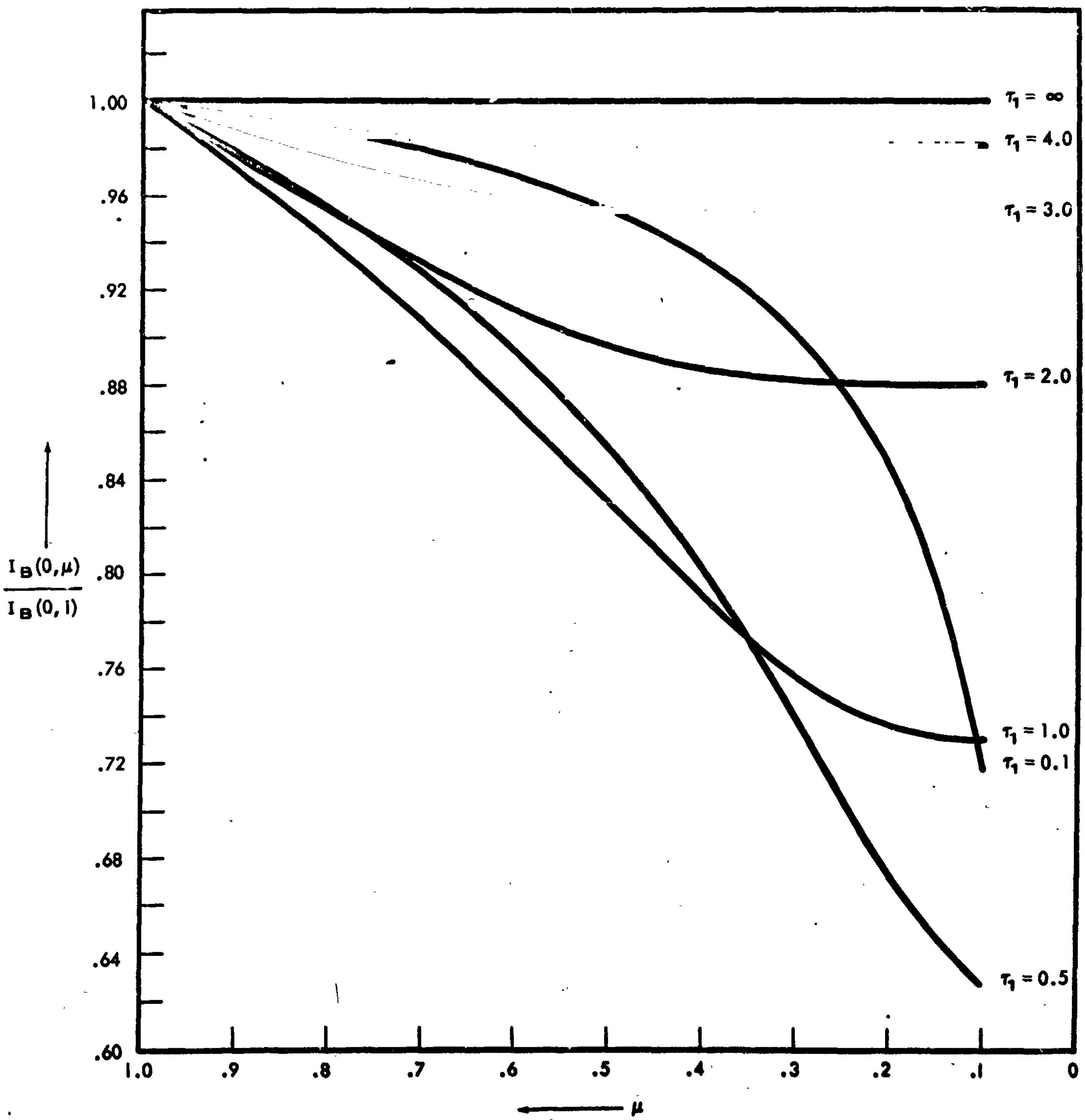

1.00
.96
.92
.88
.84
.80
.76
.72
.68
.64
.60
$\frac{I_B(0,\mu)}{I_B(0,1)}$
1.0
.9
.8
.7
.6
.5
.4
.3
.2
.1
0
μ
$\tau_1 = \infty$
$\tau_1 = 4.0$
$\tau_1 = 3.0$
$\tau_1 = 2.0$
$\tau_1 = 1.0$
$\tau_1 = 0.1$
$\tau_1 = 0.5$

Fig. 11